Regulatory variation controlling architectural pleiotropy in maize

Edoardo Bertolini[1], Brian R. Rice[2,a], Max Braud[1], Jiani Yang[1,b], Sarah Hake[3,4], Josh Strable[5], Alexander E. Lipka[2], Andrea L. Eveland[1,*]

[1]Donald Danforth Plant Science Center, St. Louis, MO 63132
[2]Department of Crop Sciences, University of Illinois, Urbana-Champaign, IL 61801
[3]Plant Gene Expression Center, USDA-ARS, Albany, CA 94710
[4]Plant and Microbial Biology Department, University of California, Berkeley, CA 94720
[5]Department of Molecular and Structural Biochemistry, North Carolina State University, Raleigh, NC 27695

*Corresponding author
[a]Current institution: Department of Soil and Crop Sciences, Colorado State University, Fort Collins, CO 80523.
[b]Current institution: Bayer Crop Science, Chesterfield, MO 63107

Abstract
An early event in plant organogenesis is establishment of a boundary between the meristem and differentiating lateral organ. In maize (*Zea mays*), evidence suggests a common gene network functions at boundaries of distinct organs and contributes to pleiotropy between leaf angle and tassel branch number, two agronomic traits. To identify developmental regulators and their sub-networks at the nexus of these two traits, we used regulatory network topologies derived from specific developmental contexts to guide multivariate genome-wide association analyses. In addition to defining network plasticity around core pleiotropic loci, we identified new transcription factors that contribute to small trait effects in canopy architecture, likely through redundancy and dose-dependency with interconnected gene family members. We also showed that structural variation in the promoter of one factor contributes to *cis*-regulatory control of pleiotropy between tassel branching and leaf angle across maize diversity. Results demonstrate the power of informing statistical genetics with context-specific gene networks to pinpoint small effect genetic loci and their *cis*-regulatory components, which can be used to fine-tune plant architecture for crop improvement.

Introduction

Plant architecture has been an important target of selection in crop domestication and improvement (J. F. Doebley, Gaut, and Smith 2006). The domestication of maize from its wild progenitor teosinte involved major architectural shifts in apical dominance and ear morphology that were pivotal in generating the backbone of a highly productive crop (Abraham-Juárez et al. 2021). Improvements to maize architecture through breeding over the last century have substantially contributed to exponential yield gains; more compact plants with upright leaves and smaller, fewer, or upright tassel branches enable increased planting densities while enhancing photosynthetic efficiency in the lower canopy (Duncan, Williams, and Loomis 1967; Duvick 2005; J. Tian et al. 2019; B. Wang et al. 2020). These architectural traits are all outputs of endogenous developmental programs, intricately connected through gene networks that we are just beginning to unravel.

Variation in plant architecture typically involves changes in placement, number, or orientation of lateral organs, which are initiated from populations of pluripotent stem cells called meristems. Often, this is regulated by meristem determinacy programs (Gaarslev, Swinnen, and Soyk 2021); recently, the concept of signaling centers acting in boundaries adjacent to meristems to modulate determinacy and diversity in grass inflorescence architecture was proposed (Whipple 2017). During organogenesis, a boundary domain is established between the meristem and differentiating lateral organs to restrict meristem maintenance and organ identity genes to their respective zones (Richardson and Hake 2018). Leaf angle (LA) in grasses is largely determined by patterning and growth of the ligule and auricles, structures that characteristically define the blade-sheath boundary and together act as a hinge to allow the leaf to recline and absorb sunlight (Richardson and Hake 2018).

Several genes expressed at initiating ligules are also expressed at the boundaries of other lateral organs, such as developing leaf primordia and tassel branches (Johnston et al. 2014; Eveland et al. 2014). Among these are *liguleless* (*lg*) *1* and *2*, which encode SQUAMOSA BINDING PROTEIN (SBP) and bZIP transcription factor (TF)s, respectively. Loss-of-function mutants in these genes have compromised ligule and auricle development, resulting in more upright leaves (Becraft et al. 1990; Moreno et al. 1997; Walsh, Waters, and Freeling 1998), but also defects in tassel branch number (TBN) and angle (TBA). Mutants in *lg2* make few to no tassel branches that are upright compared to those of normal siblings (Walsh and Freeling 1999), and *lg1* has significantly fewer branches but the phenotype is less severe than in *lg2* (Lewis et al. 2014). Several other maize mutants also show pleiotropic defects between leaf and tassel architecture traits, including those with altered brassinosteroid (BR) signaling, a plant growth hormone that modulates cell division and expansion (see Supplemental Note).

Core gene regulatory modules appear to underlie formation of a boundary, whether it is the boundary at the ligule, the boundary between leaf primordium and meristem, or between tassel branch and rachis. Similar to seminal findings in animal systems (Carroll 2008), these common modules have likely been co-opted for development of distinct tissues and underlie pleiotropy found between LA and TBN, important agronomic traits in maize improvement. Although genome-wide association studies (GWAS) have identified significant SNP-trait associations for TBN in proximity to *lg1* and *lg2*, pleiotropy between these traits are not seen extensively in natural populations (Brown et al. 2011). This is likely due to regulatory variation

within natural diversity, e.g., *cis*-regulatory elements that enable specificity in spatiotemporal patterning of gene expression and are hypothesized to be key drivers of phenotypic variation (Marand et al. 2023).

Pleiotropy is a major cause of evolutionary constraint, and regulatory variation in pleiotropic loci underpins adaptive evolution and developmental plasticity. Looking forward, the success of new technologies that allow precise engineering of genomes and pathways will depend on improving our understanding of pleiotropy in gene networks, and devising ways of dissociating pleiotropic effects during engineering crop improvement (Song et al. 2022; Hendelman et al. 2021). The pleiotropy that exists between LA and TBN in maize, and the mutants that provide a genetic framework for linking these traits, make it an ideal system for dissecting control points for context-specific gene regulation. Here, we use this system to evaluate conservation and rewiring of transcriptional networks around known pleiotropic loci in specific developmental contexts, i.e., underlying ligule and auricle development and tassel branch outgrowth. Informative network topologies from these analyses are used to guide multi-trait GWAS to gene candidates contributing to small effects in leaf and tassel architecture.

Results

A transcriptional framework for molecular explorations of tassel branching and leaf angle in maize

To delineate the gene networks underlying tassel branching and ligule development, and tissue-specific rewiring around pleiotropic loci, we leveraged a panel of maize mutants with developmental defects in TBN, LA or both, all well-introgressed into the B73 genetic background (Fig. 1a). Mutants with altered TBN and/or TBA are described in the Supplemental Note and include: *lg1*, *lg2*, *wavy auricle on blade1* (*wab1*) and the dominant *Wab1-R* allele, *ramosa1* (*ra1*), *ra2*, *brassinosteroid insensitive1* (*bri1*)-*RNAi* and *bin2-RNAi*. These genetic stocks, including B73 control plants, were grown in environmentally- controlled, high-light chambers to enable precise developmental staging of the different genotypes. Immature tassel primordia were hand-dissected immediately before and after primary branch initiation (stage 1 and 2, respectively; Extended Data Fig. 1). We also sampled across a five-stage developmental trajectory from the B73 normal tassels only, beginning with pre- and post-primary branch formation. Mutants with defects in LA included *lg1*, *lg2*, *Wab1-R*, *bri1-RNAi*, *bin2-RNAi*, and *feminized upright narrow* (*fun*), which makes a ligule but no auricles (Vajk 2019). We sampled two sections of vegetative shoot from these mutants and B73 controls, which we refer to as shoot apex 1 and 2: shoot apex 1 includes the SAM and cells that are pre-patterned to be ligule, and shoot apex 2 was taken above the meristem to include leaf primordia with developed ligules (Extended Data Fig. 1).

RNA-seq was used to profile gene expression across 140 samples (Supplementary Table 1). Principal component analysis (PCA) of the B73 normal samples showed clear separation by tissue type (i.e., tassel, SAM/pre-patterned ligule cells, and ligule-enriched), indicating distinct transcriptome profiles (Extended Data Fig. 2). Samples across the five stages of B73 tassel development revealed a continuous transcriptional gradient when plotted in PCA space. This gradient reflects progression through specific axillary meristem types, including progression from indeterminate to determinate states. Adding the mutants' transcriptome data to the PCA space also showed clear separation among tissue types and genotypes, and we

captured unique transcriptomes indicative of extreme phenotypes displayed in certain mutants (Extended Data Fig. 2).

We first examined early shifts in gene expression during primary branch initiation in the normal B73 background and observed dynamic expression of genes related to meristem identity and determinacy, organ specification, and growth hormone activity (Fig. 1b and Extended Data Fig. 3). We tested for enrichment of functional categories using Gene Ontologies (GO) within differentially expressed (DE) gene sets that were either up- or down-regulated during the shift from meristem to organ differentiation, i.e., between stage 1 and 2 tassels (1,719) and shoot apex 1 and 2 (1,858) (Fig. 1b, Supplementary Tables 2 and 4). As expected, enrichment of several GO categories shifted in common during tassel branch and ligule development, e.g., those related to meristem activity and determinacy and inflorescence morphogenesis, consistent with common sets of genes recruited for boundary establishment and organ development. GO terms related to leaf morphogenesis showed opposite expression between tissues, consistent with the leaf development program being suppressed during tassel branch outgrowth (Fig. 1b). Many plant hormone pathways were also overrepresented and tended to show different trends during tassel branch and ligule development. For example, genes related to auxin and BRs showed common expression trajectories in the two tissues, whereas jasmonic acid (JA), salicylic acid (SA) and in particular, gibberellic acid (GA), showed opposite trends (Fig. 1b). During tassel branching, members of AP2/EREB, YABBY and MADS TF families were overrepresented within DE genes (Supplementary Table 3) while Class I KNOTTED1-LIKE HOMEOBOX (KNOX) and AUXIN RESPONSE FACTOR (ARF) were highly enriched (q= 0.09e-03 and q= 0.054e-02, respectively) among down-regulated genes during ligule differentiation. ZINC FINGER HOMEODOMAIN (ZHD) and GRAS family TFs were also overrepresented during ligule development, several of which were annotated with GO terms related to GA signaling (Supplementary Table 5 and Extended Data Fig. 4).

Along the defined expression trajectory of the B73 tassel, we interpolated the mutant expression data to capture deviations along this trajectory, i.e., shifts in heterochrony. We fit a smooth spline regression model using expression values of the 500 most dynamically expressed genes across normal tassel development and used this model to classify samples relative to their transcriptomes, measured in expression time (ET) units (Fig. 1c). Expression profiles of known marker genes in maize inflorescence development (e.g., meristem identity genes) strongly support the ET classifications (Extended Data Fig. 5). Mutant expression data revealed clear differences during early organogenesis, i.e., between tassel branch initiation and development, although phenotypic differences were not observed at these stages (Fig. 1c).

For example, prominent shifts in ET classification were observed in the BR signaling mutants, *bri1*-RNAi and *bin2*-RNAi, compared to controls specifically at stage 1 but not stage 2. This indicates that transcriptional events modulated by BR signaling during tassel branch development occur early at branch initiation and become more similar to controls during branch outgrowth. The *bri1* and *bin2* genes encode positive and negative regulators of BR signaling, respectively, and the RNAi mutants display opposite phenotypes for LA and TBA (Fig. 1a; Supplemental Note). BRs happen to play an important role in maintaining boundary domain identity through control of cell division (Bell et al. 2012; Gendron et al. 2012). This is consistent with strong shifts in gene expression during primary branch initiation in tassel primordia from BR signaling mutants compared to the normal B73 controls.

The dynamic expression trajectories between stage 1 and 2 tassel primordia (i.e., showing differential shifts in expression between stages) were compared across normal B73 controls and the two BR signaling mutants; 2,236 of these genes showed a differential expression trajectory common among the mutants compared to control (Fig. 1d, Extended Data Fig. 6). These DE genes were enriched for functions related to maintenance of inflorescence meristem identity and GA biosynthesis and signaling (Fig. 1e), which were up-regulated in stage 1 tassel primordia of BR mutants compared to controls, suggesting cross-talk between BR and GA pathways. Developmentally dynamic genes that were expressed higher in BR mutants at stage 1 were also significantly enriched for ZHD TF family members ($q = 2.45^{e-03}$) (Supplementary Tables 6, 7, and 8). In addition to the common set of DE genes, the *bin2*-RNAi mutant displayed a unique set of DE genes and SBP TFs were significantly enriched ($q = 1.87^{e-02}$) among genes up-regulated in *bin2*-RNAi mutants specifically during primary branch initiation, when compared to normal plants (Fig. 1f). Among these SBP TFs were *teosinte glume architecture1*(*tga1*) and neighbor of *tga1*, which play important roles in lateral branching (H. Wang et al. 2015)

Tissue-specific gene regulatory networks reveal preservation and rewiring around pleiotropic loci in different developmental contexts

To determine transcriptional hierarchies during tassel branch and ligule development we integrated the expression data into 'tassel' and 'leaf' gene co-expression networks (GCNs) and gene regulatory networks (GRNs). A common set of 22,000 expressed genes was used to generate the two GCNs by weighted gene co-expression network analysis (WGCNA) (Langfelder and Horvath 2007). Genes were grouped based on their similar expression patterns into sixteen and eighteen co-expressed modules in 'tassel' and 'leaf' networks, respectively, which are indicated by color (Supplementary Tables 9, 10 and Extended Data Fig. 7). To assess the extent of module conservation between the two GCNs, we conducted a co-expression module preservation analysis based on a permutation method (n = 1,000; see Methods). We found that 11,221 nodes (52% of the commonly expressed genes) were statistically preserved (a = 0.05, using Fisher's exact test) and that 69% of the 'tassel' modules were conserved with one or more sub-modules in the 'leaf' GCN (Fig. 2a and Supplementary Table 11). Two 'tassel' GCN modules ("brown" and "blue") were the most preserved with more than 80% module conservation. The 'tassel' "brown" module included over-represented genes associated with regulation of meristem growth (GO:0010075, $q$value = 7.74 e^{-05}) and maintenance of shoot apical meristem identity (GO:0010492, $q$value = 0.0035) (Supplementary Table 12).

GO enrichment analysis was performed on conserved 'tassel-leaf' GCN sub-modules (Supplementary Table 13). For example, the 'tassel' "brown" GCN module included two conserved sub-modules in the 'leaf' GCN; i.e., a 'leaf' "green" sub-module (nodes = 176, Fisher's exact test $P = 5.83\ e^{-13}$) and a 'leaf' "red" sub-module (nodes = 591, Fisher's exact test $P = 0$), which were enriched for genes involved in GA (GO:0009740, q= 5.85 e^{-05}) and BR (GO:0009742, q= 0.03) mediated signaling pathways, respectively. Consistent with a mechanistic connection between BR, GA and *knox* genes (Kir et al. 2015; Bolduc and Hake 2009), the "brown-green" sub-module includes the meristem maintenance gene *knotted1 (kn1)* (Vollbrecht et al. 1991).

To visualize network rewiring within preserved sub-modules (Fig. 2b), we conducted a complementary GRN analysis to infer edge directionality. Overlaying the network connections from the GCN and GRN, we observed that several highly-connected regulatory TFs had conserved network connections in 'tassel' and 'leaf' networks. For example, ZHD15 showed a high degree of edge conservation in the "brown-green" sub-module suggesting its role as a conserved hub gene (Fig. 2b). Not surprisingly, KN1 is also predicted as a conserved hub. In contrast, the uncharacterized TF DOF25 (*Zm00001d034163*) is potentially a transient hub connected to a large number of genes in the 'leaf' GCN (*degree centrality* = 1) but fewer in the 'tassel' GCN (*degree centrality* = 0.57).

Since *lg2* mutants are strongly pleiotropic for TBN and LA phenotypes, we investigated tissue-specific connectivity of *lg2* in 'tassel' and 'leaf' GRNs. Interestingly, we observed substantial rewiring of its closest neighbor nodes with a small degree of edge preservation between 'tassel' and 'leaf', which included directed edges to *lg2* from TFs EREB92 (Zm00001d000339) and ABI41 (Zm00001d023446) (Fig. 2c). In the 'tassel' GRN, *lg2* was co-expressed with and co-regulated by several different TFs including *tassel sheath4* (*tsh4*), an interaction that was recently validated experimentally (Xiao et al. 2022). In the 'leaf' GRN, predicted regulators of *lg2* were significantly enriched for HOMEOBOX (HB) (q-value = $1.3e^{-04}$) and YABBY TFs (q-value = $2.38e^{-03}$) (Supplementary Table 14), and *lg2* was co-expressed with *lg1* as well as *liguleless related sequence1* (*lrs1*) and *sister of liguleless1*, closely related paralogs of *lg2* and *lg1*, respectively. Prior work investigating transcriptional networks at the blade-sheath boundary in maize similarly showed that these genes were all co-expressed (Leiboff et al. 2020).

Network motif analysis resolves context-specific topologies and core developmental regulators

To investigate the topology of the GRNs and interconnectedness of TFs, we annotated three-node network motifs; simple, recurrent regulatory circuits that appear in the network at higher frequency than expected by chance (Milo et al. 2002). We used information derived from directed edges inferred in the GRNs and systematically searched for three-node motifs (characterized by at least three edges) that were significantly over-represented in the 'tassel' and 'leaf' GRNs. Out of ten possible three-node motifs, three types were significantly enriched in both networks (Z score > 20) and were present at a higher concentration (≥ 10%), namely the mutual-out, regulating-mutual and feed-forward loop (FFL) (Fig. 3a and (Supplementary Table 15). To determine which TFs were predicted to be most influential in the transcriptional circuits, we ranked them based on frequency within annotated three-node motifs. We selected the top one hundred recurrent TFs from each of the 'tassel' and 'leaf' GCNs (Fig. 3b) for use in subsetting GWAS SNPs (described in below). TFs belonging to ZHD (q= 0.0028) and HB (q= 0.0002) families were the most overrepresented in 'tassel' and 'leaf' GCNs, respectively.

FFLs have been described across various organisms as local, repeated and adapted genetic circuits (Alon 2007). To gain insight into the modularity of the FFLs within our context-specific GCNs, we identified the overrepresented TFs in the two parallel regulation paths controlled by nodes "X" and "Y" (Fig. 3c). GRAS, ZHD and SBP were the most overrepresented TF families in the 'tassel' $FFL_{(X)}$ while HBs were overrepresented in the 'leaf' $FFL_{(X)}$. In both networks, these TFs were predicted to regulate several hormone biosynthesis and sugar

signaling genes, e.g., *bri1a*, *kaurene synthase3* (*ks3*), *vanishing tassel2* (*vt2*) and *ramosa3* (*ra3*).

A genomic selection approach to optimize phenotyping of maize diversity for architectural pleiotropy

We took a quantitative approach to identify loci that link TBN and LA in maize. To optimize selection for maximizing diversity in TBN and LA, a genomic best linear unbiased predictions model (GBLUP) was fit using the Goodman-Buckler diversity panel (Flint-Garcia et al. 2005) and the predicted genomic estimated breeding values (GEBVs) for TBN, LA, and ear row number (ERN), the latter included to maximize diversity for ear traits too, and first and second Principal Components of the phenotypes (PhPC1 and PhPC2, respectively) for 2,534 diverse lines in the Ames inbred panel (Romay et al. 2013) (Supplementary Table 16). Ames lines (n=1,072) were randomly selected to represent the distribution of the predicted PhPC1 and manually phenotyped for TBN and LA. Overall, the large portion of heritable variation between the selected genotypes resulted in prediction accuracies of 0.58 and 0.50 for TBN and LA, respectively. PhPC1 of the selected lines explained 56% of the total variance of TBN and LA, and was explained by trait loadings that were both positive. PhPC2 explained the remaining variance (44%) with positive (LA) and negative (TBN) loadings (Fig. 4a). Interestingly, PhPC1 explained a larger portion of the variance than either TBN or LA, suggesting that PhPC1 may be a better source for detecting pleiotropy than testing each phenotype independently.

Because plant architecture has played a key role in maize adaptation (Ross-Ibarra et al., 2007), we hypothesized that genes underlying inflorescence and leaf architecture traits would be confounded with population structure. This hypothesis was underscored by how clearly the proxy traits PhPC1 and PhPC2 subdivided the lines into their respective subpopulations (Fig. 4a). Moreover, we observed a moderate correlation (0.53) between the PhPC1 (Supplementary Table 17) and published flowering time data (Peiffer et al. 2014). These results collectively suggest divergence between TBN, LA, and their hypothetical pleiotropic regulation across maize subpopulations. Thus, the models we used in the ensuing analysis corrected for both population structure and familial relatedness (Methods).

Network-assisted multi-trait GWAS identifies gene candidates associated with TBN and LA

SNP markers were prioritized using gene sets related to TBN and LA based on network analyses (described below) and were used to guide multivariate GWAS. While this approach significantly reduced the marker density to varying degrees, we hypothesized that biological information derived from the networks could resolve novel SNP-trait associated markers.

To select genes for marker sub-setting, we generated a comprehensive GCN using the entire RNA-seq dataset (n=140) and identified sixteen modules of co-expressed genes. Using a module-feature relationship analysis in WGCNA, we identified modules that had significant correlations with tissue types, developmental stages or agronomic traits (Fig. 4b and Supplementary Table 18). For each GCN module, we estimated TBN and LA narrow-sense heritability (h^2) and compared the observed values to empirical distributions. Modules that fit the following three conditions were selected (n= 6): i) significant module-trait correlation, ii) observed h^2 values greater than the mean of their respective empirical distribution and iii) at

least 80% of genome-wide h^2 explained (Supplementary Table 19). (Fig. 4b). SNPs overlapping with genes in the selected six co-expression modules (*n*=106,790; within 2 kb upstream and downstream of the gene model) accounted for nearly all of the genome-wide h^2 associated with TBN and LA (Extended Data Fig. 8). In addition to the combined GCN, we also used a reductionist approach by selecting the top one-hundred recurrent TFs within the three-node network motifs derived from the 'tassel' and 'leaf' GRNs as an alternative way to partition SNP markers (Fig. 3b). Remarkably, SNPs (*n*=1,972) overlapping this group of genes still explained a significant portion of the genome-wide h^2, 57% and 70% respectively for TBN and LA (Extended Data Fig. 8).

For each set of markers (from combined GCN and three-node motif analysis), we conducted single-trait GWAS for LA, TBN and the first two PhPCs, and multi-trait GWAS analyses for LA and TBN. Our GWAS models collectively yielded 71 and 172 non-overlapping single trait-associated SNPs for the combined GCN and three-node motif sets, respectively (Supplementary Table 20). The majority (72%) of the trait-associated markers in the three-node motif set were associated with PhPC2, which represents opposite trait-loadings. Genes associated with PhPC2 were significantly enriched with GO terms implicated in meristem determinacy and maintenance; for example, *knotted related homeobox5* (Zm00001d035439) (Supplementary Table 21), in the 'leaf' GRN, was predicted to directly regulate *lg2* expression together with other KNOX family TFs.

Overall, the multivariate analysis with the two marker sets identified a total of 23 potential pleiotropic loci that hosted (or in close proximity to) SNPs simultaneously associated with both LA and TBN phenotypes (Fig. 4c and Supplementary Table 22). Two of these SNPs were in common between analyses with the two marker sets indicating high-confidence associations that may contribute to phenotypic pleiotropy. Both SNPs were located within genes encoding TFs; one located in the last exon of *ereb184* (Zm00001d034204), an ortholog of *AINTEGUMENTA1* in *Arabidopsis thaliana*, known to control plant growth and floral organogenesis.(Liu et al. 2020), and one in the last exon of *zhd21* (Zm00001d041780), which was previously shown to express in leaf primordia during ligule initiation (Leiboff et al. 2020). These two markers were also associated with TBN in the single-trait GWAS. Also in the single-trait GWAS, the marker in ereb184 associated with PhPC1, reinforcing the notion that PhPC1 may be used to detect pleiotropic loci.

We found that *ereb184* and *zhd21* were connected in the leaf GRN through four TFs: *ereb93*, *zhd20, zhd16* and *barren inflorescence2*; the latter regulates tassel branch outgrowth in maize (McSteen et al. 2007). Predicted downstream targets of these two TFs suggest that they regulate architecture traits through different but interconnected developmental circuits made of *knox* genes and genes regulating hormone metabolism, transport and signaling, especially involved in auxin, GA and BR pathways (Fig. 4d and Supplementary Table 23). The link between *ereb184* and *zhd21* was also supported by statistical epistasis analysis (Extended Data Fig. 9 and Supplementary Table 24), which highlighted their interaction together with other TFs and members of the ZHD family, such as *zhd1, zhd12 and zhd15*.

Maize network data can be used to guide explorations of SNP-trait associations in sorghum

We further tested whether the small set of markers selected based on three-node network motifs in maize was sufficient to guide GWAS to candidate SNP-trait associations for LA in sorghum. Among the maize genes within the motif set, we identified 142 sorghum orthologs and their associated SNPs from the Sorghum Association Panel (SAP) (Casa et al. 2008). Using the selected SNP markers together with publicly available LA phenotype data for the SAP (Mantilla Perez et al. 2014), we first tested h^2 for this trait and found that variation in these genes explained more than 60% of the sorghum genome-wide LA h^2 (Fig. 5a). Therefore, we conducted a single-trait GWAS for LA. Eight sorghum LA-associated markers were found within genic or proximal regulatory regions of seven genes (Fig. 5b and Supplementary Table 25), including maize orthologs of *nac112* (*Sobic.009G143700*), *ofp39* (*Sobic.008G042200*), *c3h16* (*Sobic.006G256500*) and *Zm00001d026535* (*Sobic.006G254500*), which were also identified in maize single-trait GWAS for PhPC1, PhPC2 and/or TBN. Additionally, a significant SNP was identified within the maize ortholog of *ereb114* (*Sobic.002G022600*), a paralog of maize *ereb184*. Based on first neighbors connectivity in the maize leaf network, *ereb114* is situated either up- or downstream of known *knox* genes involved in meristem maintenance and axillary meristem formation in maize, e.g., *kn1*, *gn1*, *rs1* and *lg4*, suggesting conservation of developmental circuits controlling LA between maize and sorghum (Fig. 5c). Furthermore, *ereb114* is predicted to directly target *zhd21*, another high-confidence gene candidate from the multi-trait GWAS for LA and TBN.

***zhd* genes regulate leaf and tassel architecture in a dose-dependent manner with functionally redundant family members**

Throughout this study, genes encoding ZHD TFs repeatedly emerged as important players in ligule and tassel branch development. These TFs appear as putative hubs in the networks or highly connected to known developmental pathways. *zhd* genes are enriched within BR signaling-responsive genes during early development, and one was identified as a high-confidence candidate gene in multi-trait GWAS for TBN and LA. To test whether disruption of network candidate *zhd* genes have a phenotypic effect on tassel and/or leaf architecture, we studied the effects of independent *Mutator* (*Mu*) transposon insertions in the coding region of *zhd21* and *zhd1* (UniformMu, Methods). We did not observe differences in TBN or LA in the single mutant alleles, perhaps due to genetic redundancy Extended Data Fig. 10. However, genetic interactions between *zhd1* and *zhd21* revealed pleiotropic shoot phenotypes that included dose-dependent phenotypic effects on tassel branching and leaf architecture. The strongest phenotypic effects were observed in *zhd1/1;zhd21/+* plants where TBN and LA (exterior angle) were significantly enhanced (Wilcoxon *p*-value TBN= 0.0094, LA= 0.0008) (Fig. 6a,b). The resulting genetic interactions between *zhd1* and *zhd21* indicate redundant, yet sub-functionalized roles for these genes in controlling both architectural traits.

***Cis*-regulatory elements and structural variation around *ereb184* modulate pleiotropy in TBN and LA**

Our gene candidate *ereb184* was also among the top hundred recurring TFs within 'leaf' GRN three-node motifs and positioned as a regulatory factor in many FFLs ($FFL_{(x)}$; 7,422). Notably, these FFLs were overrepresented by ZHDs at the $FFL_{(y)}$ node. We found that *ereb184*-regulated FFLs potentially regulate a set of downstream genes ($FFL_{(z)}$) associated with functional

categories that overlapped with those enriched during tassel branch and ligule development (Fig. 7a and Supplementary Table 26). In particular, four KN1-regulated FFLs highlighted *ereb184* connections to homeotic genes *rough sheath1*, *gnarley1* and *zea floricaula1* and *2* that were detected in the leaf network as directly targeting *lg2* (Fig. 7b).

Scanning the gene regulatory space around *ereb184,* we observed approximately 100 kb of intergenic sequence upstream of the TSS. We integrated various publicly available omics' datasets to investigate potential regulatory regions (see Data accessibility). We identified three genomic regions with regulatory signatures including unmethylated marks, which colocalized with conserved non-coding sequences and showed increased nucleotide diversity, similar to that overlapping the coding region of *ereb184* (Fig. 7c). To investigate tissue-specific chromatin accessibility, we generated Assay for Transposase-Accessible Chromatin (ATAC)-seq data from the B73 shoot apex 2 tissue (including developed ligules) and compared the profiles in this region to publicly available ATAC-seq data from tassel primordia. All three regulatory regions showed tissue-specific chromatin signatures that overlapped with other epigenetic marks, highlighting potential tissue-specific regulation proximal to *ereb184*. Overlaying publicly available chromatin interaction data (Hi-C) from maize indicated potential chromatin looping between the *ereb184* promoter and one of the upstream intergenic regions (Fig. 7c).

Using public data from the maize Nested Association Mapping (NAM) Consortium (Hufford et al. 2021), we identified a structural variation (SV) of approximately 5 kb in the promoter region of *ereb184*. Based on resequencing data of the 26 NAM founder lines, this SV was either present or absent, and mainly absent in the tropical inbred lines. We also observed tissue-specific chromatin accessibility adjacent to the SV, suggesting it could be located within a regulatory region. We tested whether presence/absence variation (PAV) of the SV in the promoter of *ereb184* had an effect on pleiotropy between LA and TBN. In addition to the NAM founder reference genomes, we extended the analysis to include 231 accessions that we phenotyped from the Goodman-Buckler panel (Flint-Garcia et al. 2005), incorporating existing sequencing data (B. Song et al. 2021) to define PAV. Strikingly, we found that maize lines without the SV showed increased TBN and more upright leaves, while lines with the SV showed the opposite trend, and these results were significant by Wilcoxon rank-sum test (p-values TBN= 0.0078, LA= 0.043) at $\alpha = 0.05$. Also, based on transcriptome data from the NAM Consortium, founder lines with the SV present in the *ereb184* promoter had lower gene expression (Wilcoxon rank-sum test p=0.029) in shoot tissue (Fig. 7c).
These results suggest that SV in the promoter of *ereb184* contributes to the regulation of these pleiotropic, agronomic traits.

Discussion

In maize, mutants that affect the ligule also affect tassel branch initiation ((Johnston et al. 2014; Eveland et al. 2014)) and genes expressed at initiating ligules are also expressed at the boundary of other lateral organs ((Johnston et al. 2014; Eveland et al. 2014)) such as tassel branches. In this study, we leveraged this well-characterized maize genetics system to investigate the molecular underpinnings of pleiotropy: network rewiring around pleiotropic loci in two developmental contexts, the redeployment of TFs for analogous but different developmental processes, and *cis*-regulatory variation proximal to pleiotropic loci. By strategically integrating context-specific biological data, e.g., GRNs tailored to capture gene regulation underlying tassel

branching and leaf architecture traits, and multivariate GWAS models exploiting maximal diversity in TBN and LA, we identified new regulatory factors that contribute to architectural pleiotropy in maize. Our approach demonstrates potential for identifying loci with small effects on multiple traits and can be applied in any genetic system to disassociate pleiotropic phenotypes through manipulation of *cis*-regulatory components and gene network connections.

Pleiotropy, the effect of a gene on multiple phenotypic characters, is one of the major forces that shapes and constrains biological evolution. Pleiotropy in crop phenotypes can also limit productivity ceilings. For example, selection on a certain desired phenotype may come with unintended deleterious manifestations of another. This can happen when a gene controlling a target trait also functions in another developmental or physiological context. In recent years, the dramatic production gains of the 20th century have plateaued in the world's most important cereal crops (Grassini, Eskridge, and Cassman 2013). Looking forward, step changes in crop improvement and sustainability will rely on targeted manipulation of regulatory pathways underlying agronomic traits so they can be fine-tuned for enhanced plant productivity and resilience in dynamic environments (Bailey-Serres et al. 2019; Eshed and Lippman 2019). Central to this is the ability to predict and design highly-specific genetic changes at pleiotropic loci with minimal perturbation to the complex networks in which they reside. This will require a comprehensive knowledgebase of the regulatory networks underlying traits of interest and how they interface across whole plant development and physiology.

A well-established principle of developmental evolution is that genes are reused in different developmental processes leading to pleiotropic effects (Carroll 2005). Evolution of morphology is largely due to spatiotemporal changes in expression of functionally conserved proteins. These changes often occur through mutations in *cis*-regulatory elements associated with pleiotropic developmental loci (Carroll 2008; Marand et al. 2023). Genetic diversity thus reduces pleiotropy by introducing *cis*-regulatory variation, which can help fine-tune context-specific gene expression. For example, variation in *cis*-regulatory elements can facilitate re-deployment of gene modules in new developmental contexts (Doebley and Lukens 1998; Wittkopp and Kalay 2011). With respect to crop improvement, manipulation of these elements at functionally conserved pleiotropic loci would allow for greater precision in engineering or breeding optimal plant ideotypes.

In comparing predicted gene regulatory interactions between tassel branch and ligule development, both conservation and rewiring of the GRNs were observed. In one preserved sub-network that was highlighted in Fig. 2b, KN1 and ZHD15 were maintained as hubs with conserved regulatory connections in both developmental contexts. Conservation around KN1 was not surprising given it is a master regulator of meristem maintenance. Identifying ZHD15 as a hub was novel, but also consistent with other lines of evidence from this study that implicate ZHDs as central players in architectural pleiotropy between leaf architecture and tassel branching. On the other hand, there was extensive rewiring of predicted network connections around LG2, which strongly controls LA and TBN in a pleiotropic manner. This suggests that the re-deployment of LG2 in different developmental contexts was accompanied by loss and gain of regulatory connections to gene targets and targeting TFs. Perhaps LG2 provides a common function in setting up boundaries and its interactions with context-specific sub-networks shape the specific developmental programs.

We showed that these biological context-specific networks could be used to subset markers for multi-trait GWAS and identify new loci that contribute to architectural pleiotropy in LA and TBN. Using two different network-guided approaches we identified several gene candidates in and around significant SNP-trait associations. Strikingly, both approaches identified significant SNPs within two of the same TF-encoding genes, *zhd21* and *ereb184.* Both TFs are members of large families that are largely uncharacterized in maize. Interestingly, our network predictions showed that these two TFs were closely linked in gene regulatory space and were also highly interconnected with other ZHD family members (Fig. 4d). Consistent with network interconnectedness among ZHDs, we showed that influence on tassel branch and leaf architecture by *zhd21* mutant alleles is visible only in combination with mutations in another family member, *zdh1*. This highlights redundancy and network connectedness within these larger TF families to allow for fine-tuning of gene expression and output phenotypes.

Network predictions also indicated that *ereb*184 and ZHD family members were highly interconnected with known *knox* genes, which are fundamental players in organogenesis. For example, EREB184 is predicted to participate in several FFLs with KN1 and other KNOX TFs, which connect it to regulation of *lg2*. Direct targets of KN1 in these FFLs were previously validated by ChIP-seq data (Bolduc et al. 2012). Notably, several GA biosynthesis genes were predicted as direct targets of ZHD21 in the ZHD21-EREB184 sub-network space. This is consistent with our data showing functional enrichment of GA pathways in both developmental contexts and among genes DE in tassel primordia of BR signaling mutants during primary branch initiation; *zhd* genes were significantly enriched among these DE genes, providing regulatory links between the two growth hormones.

The vast stretch of intergenic space (~100 kb) upstream of *ereb184* is sprinkled with regulatory signatures, including tissue-specific accessible chromatin regions, which potentially regulate its context-specific expression. The structural variation (SV) in its upstream promoter region, which is present in approximately half of the NAM founders, appears to control expression of *ereb184*; expression levels are significantly different in NAM lines with the SV compared to those that don't. Presence or absence of the SV may contribute to differences in spatiotemporal expression patterns of *ereb184* and could underlie the shifts in pleiotropy between LA and TBN. The origin of this SV is unclear. A blast search of the SV DNA sequence against a curated transposable element database revealed the presence of a probable LTR Gypsy retrotransposon (86% alignment identity) in the 3-prime region of the SV toward the TSS of the gene, as well as interspersed Helitron fragments. Differential chromatin accessibility between tassel primordia and shoot apex was evident in a regulatory region immediately proximal to the SV. Perhaps the SV is disrupting TF-binding interactions at this site in the *ereb184* promoter or even interfering with long-range regulation through chromatin looping as suggested by a proximal Hi-C interaction.

Small effect loci for target traits are difficult to pinpoint with GWAS given that large trait effects generally dominate, which is compounded by the threshold for significance rising with marker density due to multiple correction. Targeted GWAS with a limited, but biologically informed marker set, has been demonstrated using pathway enrichment analysis (Lipka et al. 2013) and chromatin accessible regions (Parvathaneni et al. 2020). Application of these methods to identify informative smaller SNP sets can enhance genomic predictions. Here, we showed that even SNP subsets identified with small numbers of genes prioritized through

network analyses not only produced heritabilities similar to a genome-wide set of markers, but also enabled detection of small effect loci that were validated to have effects on tassel and leaf architecture. We further showed that the context-specific networks from maize could be used to inform GWAS in closely related sorghum. The analysis in sorghum identified *ereb114*, a paralog of *ereb184*, which was connected to it and *zhd21* in the network.

Our analyses support the utility of biologically informed, context-specific networks for guiding GWAS in various applications and for identifying loci that connect phenotypic traits. Results highlight various mechanisms by which expression of pleiotropic trait phenotypes are modulated, including through network interconnectedness of redundant TF family members or SV in *cis*-regulatory components. We anticipate that this approach can be used widely to identify pleiotropic loci for manipulation for crop improvement.

Methods

Plant material for RNA-seq experiments

Mutants were introgressed at least five times into the maize B73 inbred. All were grown along with B73 controls in environmentally controlled growth chambers at the Danforth Center Integrated Plant Growth Facility with 14 hr days, 28° C / 24° C, 50% humidity and 450 µMol light. Plant materials were sown in cone trays (5 cm diameter, 11.5 cm depth, 142 ml total volume) in a Metromix 360-turface blend. At 14 Days After Sowing (DAS), seedlings were transplanted to larger pots (27 cm diameter, 24 cm depth, 14 L total volume; three plants per pot) with Berger 35% soil and 10 g of corn top dressing. Prior to tissue sampling, development of tassel primordia was tested and staged for uniformity across the different genotypes. Plants were staggered across a two week time period for tissue collections in identical conditions.

Tissue sampling and RNA extraction

Tassel primordia were hand-dissected and flash-frozen in liquid N. For each genotype, fifteen primordia were pooled per replicate for stage 1 and ten for stage 2 (Extended Data Fig. 1). Shoot apex 1 and 2 were collected by cutting plant near the base and within the plant to leave ~10 cm section of tissue. For shoot apex 2, whorls were removed one by one until reaching a leaf where the developing ligule was less than ~.75cm from that leaf's node. The leaf was then carefully removed, tearing away from its node. A section of tissue~1mm above and below developing ligule was excised using a razor blade and flash frozen. This process was repeated for 2-3 additional whorls, each successive ligule being less developed and closer to its node. 3-4 ligule sections were cut per plant, with 2-3 plants being pooled together in a tube. Following completed dissection of shoot apex 2, shoot apex 1 was collected by using a razor blade to excise 2mm section of tissue to include the shoot apical meristem and any surrounding leaf whorls.

For each tissue type and developmental stage, four biological replicates were collected. Tissue samples were ground using a bead shaker with liquid nitrogen in a 2 ml tube with a 5 mm ceramic bead. RNA isolation from tassel material was performed using the PicoPure RNA isolation kit (ThermoFisher Scientific) according to manufacturer's instructions with the following adjustments: 40 µl and 60 µl of RNA extraction buffer were added respectively to stage 1 and stage 2 ground tassels. After 30 min incubation at 42°C, samples were centrifuged at 800 g for 2 min. Equal volume of 70% EtOH was added to samples and processed according to kit

directions. On-column DNase I treatment was performed per instructions using RNase-Free DNase I kit (Qiagen) to remove residual DNA.
RNA isolation from shoot apex samples was performed using the Zymo quick-RNA plant kit according to manufacturer instructions with the following adjustments: Lysis buffer was added directly to the ground tissue and centrifuged, supernatant was added directly to the filtration column. DNase I treatment was performed using the supplied DNase I enzyme according to manufacturer instructions.
All RNA quality was quantified using the NanoDrop One Spectrophotometer (Thermo Fisher Scientific) and using the RNA-6000 Pico chip from (Agilent) to ensure RNA integrity.

RNA-seq libraries, sequencing and data analysis
Poly(A)$^+$ RNA-seq library preparation and sequencing were outsourced to Novogene (USA). Libraries were multiplexed 12 per lane and sequenced using the Illumina HiSeq4000 platform with a 150-bp paired-end design. On average for each sample we generated more than 60 million paired-end reads with quality score (Phred-score) > 30.
Raw reads were processed to filter out low quality reads, adaptors or barcode remnants using the program *Cutadapt* v2.3 (Martin 2011) and the wrapper tool *TrimGalore* v0.6.2 (http://www.bioinformatics.babraham.ac.uk/projects/trim_galore/) with default parameters except for --length 70 --trim-n --illumina. Clean reads were used to quantify the maize B73 AGPv4 gene models with *Salmon* v1.4.0 using the selective alignment method with a decoy-aware transcriptome (Srivastava et al. 2020). A Salmon index was created using default parameters from the cdna fasta file (Zea_mays.AGPv4.cdna.all.fa) together with the genome reference fasta file (Zea_mays.AGPv4.dna.toplevel.fa) to generate the decoys for the selective alignment method. Maize reference files were downloaded from Ensembl Plants release 34 (ftp://ftp.ensemblgenomes.org/pub/plants/release-34/fasta/zea_mays/).
Briefly, clean reads were mapped to the reference transcriptome using *Salmon quant* command with default parameters except for the options -l A --numBootstraps 100 --validateMappings. Expression levels were imported in R using the Bioconductor package *tximport* (Soneson, Love, and Robinson 2015), summarized to gene level using the function *summarizeToGene()* and presented in TPM (Transcript Per kilobase Million).
Overall gene expression levels between replicated samples (n=4) were highly related with correlation coefficients $r \geq 0.92$.
Differential expression analysis was performed using the Bioconductor package DESeq2 (Love, Huber, and Anders 2014). Specific pairwise contrasts were applied to compare mutant genotypes against the equivalent wild-type sample. To test differences along the developmental gradient associated with tassel branching attributable to a given genotype in comparison with B73, we set up an interaction design formula: ~ Genotype + Tissue + Genotype:Tissue. Genes were considered differentially expressed based on false discovery rate ≤ 0.05. To standardize the relative expression of each gene across the three genotypes (*bin2*, *bri1*, B73 control), we normalized the expression values for each gene within the triad as follows: relative expression $bin2_{gene(i)}$ = TPM ($bin2_{gene(i)}$) / TPM ($bin2_{gene(i)}$) + TPM ($bri1_{gene(i)}$) + TPM ($B73_{gene(i)}$); relative expression $bri12_{gene(i)}$ = TPM ($bri1_{gene(i)i}$) / TPM ($bin2_{gene(i)i}$) + TPM ($bri1_{gene(i)i}$) + TPM ($B73_{gene(i)i}$); relative expression $B73_{gene(i)}$ = TPM ($B73_{gene(i)}$) / TPM ($bin2_{gene(i)}$) + TPM ($bri1_{gene(i)}$) + TPM ($B73_{gene(i)}$).

Expression time was calculated using a smooth spline regression model (Eilers and Marx 1996) with the R function *bs()*. We fitted a b-spline (3-knot with three degrees of freedom) modeled on the first and second principal component of the 500 most dynamically expressed genes across normal tassel development. Data points from mutant backgrounds were classified based on their location on the spline in relation to this model.

Gene network analyses

Gene co-expression networks (GCNs) were built using the R package *WGCNA* (v.1.68) (Langfelder and Horvath 2008). Expression data of protein coding genes were imported into R with the function *DESeqDataSetFromTximport()*. For each GCN we selected expressed genes based on row mean > 5 counts with the R function *rowMeans()* and normalized the count expression level of each gene according to the variance stabilizing transformation (VST) with the function *vst()* from *DESeq2* package. The Pearson correlation was used to select samples for the gene co-expression networks. Highly correlated biological replicates with $r \geq 0.92$ were retained and independently input in the network analyses. Based on the correlation coefficient, only one sample derived from the *lg1-R* stage 1 tassel (replicate 2) was excluded from the network analyses.

We calculated the soft power threshold as the first power to exceed the scale-free topology fit index of 0.9 for each network. The soft power was set to 6 for individual tassel and leaf networks and to 7 for the combined network. Module detection was calculated via dynamic tree cutting using the function *blockwiseModules()* with the following parameters: type = signed, corType = bicor, minimum module size = 30, mergeCutHeight = 0.25. The parameter maxBlockSize for each network was set equal to the total number of expressed genes passing the row mean cutoff as described above; 22,499 and 22,716 respectively for the 'tassel' and 'leaf' networks. The topographical overlap matrix (TOM) was calculated for each network using the function *TOMsimilarityFromExpr()* with parameters matching those used in the module detection for each network. Networks were exported with the function *exportNetworkToCytoscape()* with the following parameters: weigh t= TRUE and threshold = 0.00. The R package *igraph* v1.2.4.1 *(Csardi and Nepusz 2006)* was used to build graphs from the exported networks with the function *graph_from_data_frame()* and to calculate the graph statistics.

Preserved GCN modules between the tissue specific networks were computed using the function *modulePreservation()* with 1,000 permutations and the gene sub-module preservation between the networks was calculated using the R package *GeneOverlap* (v.1.28).

For the GCN generated from combined tassel and shoot apex samples, the module-to-sample association analysis was conducted evaluating the correlation between the module eigengene and samples of different developmental groups: i) tassel primordia at stage 1, ii) tassel primordia at stage 2, iii) shoot apex 1 and iv) shoot apex 2. In addition, we tested associations between module eigengene and three traits of interest: leaf angle (LA), tassel primary branch number (TBN) and tassel branch angle (TBA). We created a metafile where samples were categorized according to the four sample groups and three traits. The R function *cor()* and *corPvalueStudent()* were used to test the correlation between the module eigengene and the variables. Modules with $r > |0.8|$ were considered strongly correlated.

For the context-specific gene regulatory networks (GRNs), a machine learning approach was applied to predict targets of maize known TFs using the Bioconductor package *GENIE3* (Huynh-

Thu et al. 2010). Maize TFs were downloaded from the GRASSIUS repository (www.grassius.org) and overlapped with the expression matrices. TFs were set as “regulators” to infer their “targets” based on the gene expression abundance. The *GENIE3* algorithm was run with the following parameters: treeMethod = "RF", nTrees = 1,000 and putative target genes were selected with a weight cutoff ≥ 0.005.
GRNs were used to identify three-node sub-graph motifs between genes. To determine which three-node sub-graphs were significantly enriched in the GRNs, we scanned for all possible three-node sub-graphs and compared results with a set of randomized networks (n = 1,000) with the same characteristics. This analysis was conducted with the R package *igraph* v1.2.4.1 using the following functions: *graph.full()* with n equal to the number of genes in the tissue-specific GRNs*, triad.census()*, *cliques()* with min and max set to 3. Motif significance was determined by comparing the number of observed motifs with the number found in the randomized networks. Genes involved in the fully connected three-node sub-graphs were selected and ranked based on their frequency.

Transcription Factor and Gene Ontology enrichment analysis
Maize TF and GO annotations were downloaded from GRASSIUS (www.grassius.org) (Burdo et al. 2014) and GOMAP (doi.org/10.7946/P2M925) (Wimalanathan and Lawrence-Dill 2021), respectively. The enrichment analysis was conducted with the Bioconductor package clusterProfiler (Yu et al. 2012) using the function *enricher()* with default parameters and cut-off of q = 0.1, where q is the p-value adjusted for false discovery rate using the Benjamini-Hochberg correction. GO term annotations were downloaded from the database QuickGO (https://www.ebi.ac.uk/QuickGO/).

Germplasm selection and genotype data
A training set of 281 genotypes from the Goodman-Buckler diversity panel (Flint-Garcia et al. 2005) was used to predict upper leaf angle (LA), tassel branch number (TBN), ear row number (ERN) and their corresponding principal components (PhPC1, PhPC2, PhPC3) in the Ames inbred diversity panel (a.k.a. the North Central Regional Plant Introduction Station (NCRPIS) panel) (Romay et al. 2013). First, using publicly available multi-locations phenotypic data for the Goodman-Buckler panel (Brown et al. 2011; F. Tian et al. 2011), we fit a linear model with environment and genotype as fixed effects from which we obtained the best linear unbiased predictions (BLUPs) for each individual. The PCs of the three phenotype BLUPs, and all further phenotypic (Ph)PCs, were produced using the R function *prcomp()*. Data were centered and scaled before PhPC analysis. The genotype BLUPs of Goodman-Buckler panel phenotypes and PhPCs were used to train a genomic best linear unbiased prediction (GBLUP) (VanRaden 2008) model that obtained predicted genomic estimated breeding values (GEBVs) for 2,534 individuals in the Ames panel. Models for BLUPs, GBLUPs and GEBVs were conducted in R with the package *ASReml-R* (Butler et al. 2017). Kinship matrices for GBLUP were produced according to the description in the ‘Heritability’ section below.
Genotypic data for the two diversity panels were downloaded from Panzea (www.panzea.org) and filtered for indels and non-biallelic markers. Missing data were imputed with the nearest neighbor method where distance is defined as linkage disequilibrium between two SNPs (Money et al. 2015). SNPs with low minor allele frequency were filtered using a 0.01 cut-off.

Prior to analysis, genotypes used in this study were converted to AGPv4 coordinates using the tool CrossMap v0.3.7 (Zhao et al. 2014) with the chain file from Gramene release 61 (Jiao et al. 2017).
Nucleotide diversity, the average pairwise difference between all pairs of genotypes (Nei and Li 1979), was measured for each SNP using all genotypes for which GBS data were available. Marker filtering and nucleotide diversity calculations were achieved using *VCFtools* (Danecek et al. 2011)

Phenotypic data collections

Phenotypic data collection was conducted at the University of Illinois, Urbana Champaign over three years (2018-2020). Each year, 425 Ames panel lines were randomly selected from across the distribution of the predicted PhPC1 values and planted. In addition, 75 lines from the Goodman-Buckler panel were planted (same lines each year) to ensure consistency across years. Lines were planted as single-row plots in mid May each year; 28,000 seeds per acre with 30-inch row spacing. Field design was a randomized complete block design with two replicate blocks per year. Phenotypic observations were conducted during the first week of August after the majority of genotypes had flowered. Measurements of LA were taken from the leaf immediately above the uppermost ear. If no ear was present, we selected the fifth leaf below the flag leaf. Only plants with emerged tassels were phenotyped. The angle was measured from beneath the leaf from the horizontal axis, i.e., the stalk, to the midrib. An angle of 90° would indicate an entirely upright leaf, and an angle of 0° would be perpendicular to the stalk. TBN was conducted by counting every branch that originated from the tassel rachis. For each genotype three representative plants per plot were measured.
For each trait, we applied the mixed linear model to obtain BLUPs for each genotype:

$$Yijk = \mu + Gj + Ej + Bk(j) + \epsilon ijks \quad (3)$$

where, the phenotype (Y) is explained by the ith genotype (G) observed in the kth block (B)) nested in the jth year (E). Individual plants within a plot are considered subsamples (s).
After removing outliers, BLUPs for 1,064 and 1,072 genotypes for LA and TBN, respectively, were obtained.

Heritability

Prior to estimating heritability ($\hat{h}^2$), SNP partitions were pruned with Plink 1.9 (Chang et al. 2015) to remove markers in LD of 0.7 or greater within a 50 bp window. The window was shifted five-bps and pruning repeated. For a given pruned SNP partition, a kinship matrix K was produced with the following model,

$$K = \frac{XX'}{n_p} \quad (4)$$

where X is the normalized SNP matrix, X' is its transpose, and n_p is the number or SNPs in the given partition. Narrow sense heritability $(\hat{h}^2)$ is estimated as $\frac{\widehat{\sigma_G}^2}{\widehat{\sigma_P}^2}$ where $\widehat{\sigma_G}^2$ is the additive genetic variance estimate and $\widehat{\sigma_P}^2$is the total phenotypic variance from model (2) when fitted

using REML (Gilmour, Thompson, and Cullis 1995; Lee and van der Werf 2006). We generated null distributions by estimating $\hat{h}^2$ for 1,000 random gene sets using the SNPs found within their proximal regulatory region (± 2 Kb from TSS and TTS). Random sets had an equal number of genes compared to the partition being tested. Genes in a given partition were removed from the entire genome-wide set before random selection. The software LDAK (Speed et al. 2017) was used to produce kinship matrices and estimate $\hat{h}^2$.

Marker subsetting based on network analyses

Genomic coordinates of gene sets derived from network analysis approaches (those from select co-expression modules and those most highly connected in three-node sub-graphs) were retrieved and imported in R. We used the Bioconductor package *GenomicRanges* (Lawrence et al. 2013) to select makers within the genomic windows defined as ± 2 kb from the TSS and the TTS of the co-expressed genes. Marker coordinates were intersected with the gene coordinates using the function *findOverlaps()* with the options type = within, ignore.strand = T.

Genome-wide association studies

We conducted single- and multi-trait association studies for LA and TBN. Single trait associations were conducted using Bayesian-information and Linkage-disequilibrium Iteratively Nested Keyway (BLINK) (Huang et al. 2019) conducted in GAPIT (Lipka et al. 2012). Before testing SNPs, the Bayesian information criteria (BIC) (Schwarz 1978) was used to select the models with the optimal number of PCs using the Ames panel genome-wide pruned SNP dataset.

To test for pleiotropic associations, we utilized two approaches: i) BLINK, where the response variable was either the first or second PhPC of LA and TBN (PhPC1, PhPC2); and ii) multivariate extension of MLM (mvMLM), where the response was an *n*-by-*t* matrix with *n* being the number of observations and *t* the number of traits (Rice, Fernandes, and Lipka 2020) conducted in GEMMA (Zhou and Stephens 2014). For mvMLM we conducted a leave-one-chromosome-out kinship approach (Chen and Lipka 2016). Since kinship was chromosome specific the BIC optimal number of PCs was considered on a chromosome specific basis. Multiple testing correction was conducted based on the number of SNPs in a given partition using the Benjamini & Hochberg false discovery rate (FDR) procedure (Benjamini and Hochberg 1995). Genes with SNPs with an FDR-adjusted P-value below 0.2 were considered for further analysis.

Statistical analysis of *ereb184* genetic interactions

We tested for epistatic interactions by modifying the unified MLM as follows:

$$Y = Q\gamma + S_1\alpha_1 + S_2\alpha_2 + S_1S_2\beta + Z\mu + \varepsilon$$

where $\boldsymbol{Y}$ is *n* vector of phenotype BLUPs with *n* being the number of observations; $\boldsymbol{Q}$ is the *n-by-(p+1)* incidence matrix corresponding to the intercept, as well as *p* fixed effect covariates (i.e., principal components) accounting for subpopulation structure; S_1 is an *n-by-1* incidence vector for the peak associated SNP from *ereb184*; S_2 is an *n-by-1* incidence vector for the testing SNP and S_1S_2 their interaction; α_1 is the additive effect of the peak associated SNP; α_2 is the additive effect of the testing SNP; β is the additive x additive epistatic effect between the peak

associated SNP and the testing SNP; $\boldsymbol{Z}$ is an *n-by-n* incidence matrix relating u to $\boldsymbol{Y}$; $\mu \sim N(0, 2K\sigma_G^2)$; and $\varepsilon \sim MVN(0, I\sigma_e^2)$ is the residual error with variance with *I* being the identity matrix and σ_e^2 the residual variance. The peak-associated SNP and the testing SNP are treated as fixed effects. The model was performed so that S_2 was a SNP assigned to a motif gene and run for each SNP in the motif gene partition including those assigned to *ereb184 that were not* S_1. The model was run in *ASReml-R* (Butler et al. 2017).

Sorghum LA association study

We retrieved sorghum orthologs based on (Zhang et al. 2017), which identified 11,000 sorghum-maize syntenic orthologs (https://figshare.com/articles/dataset/Grass_Syntenic_Gene_List_sorghum_v3_maize_v3_4_with_teff_and_oropetium_v2/7926674/1). Of the 200 maize TFs within our top-ranked network motif connectedness, we identified 158 sorghum-maize syntenic orthologs. Sorghum BTx623 reference (version 3) gene coordinates were retrieved from the GFF Sbicolor_454_v3.1.1.gene.gff3 (Phytozome v12.1). Sorghum has larger LD blocks than maize (Morris et al. 2013) therefore for each sorghum-maize syntenic ortholog, we extended the gene coordinates of ±10 kb from TSS and TTS, respectively using the R package *GenomicRanges* and the function *start()* and *end()*. These sorghum orthologs with extended coordinates were used to subset proximal makers using the Bioconductor function *findOverlaps()* with the option type="within" and ignore.strand=T.

Sorghum LA phenotype data were previously collected for 296 individuals from the Sorghum Association Panel (SAP) (Casa et al. 2008) from the leaf below the flag leaf (Mantilla Perez et al. 2014). SAP GBS data (Bouchet et al. 2017) were filtered at MAF 0.05. All analyses in sorghum were conducted according to the methods described above for maize.

Analysis of *zhd* UniformMu insertion lines

Maize plants were grown at North Carolina State Method Road Greenhouse under 16 hours of supplemental light/8 hours dark, and relative temperatures of 29.4°C day and 23.9°C night, and 12 inch pots in Metro-Mix 830-F3B (SunGro Horticulture).

The *zhd1-Mu2277*(Mu ID: mu1022277, AGPv4 coordinates: Chr4:12135894-12135902) and *zhd21-Mu8735* (Mu ID: mu1018735, AGPv4 coordinates Chr3:137588828-137590836) alleles were isolated in W22 inbred lines carrying exonic Mutator (Mu) transposon insertions as part of the UniformMu transposon collection (McCarty et al. 2005).

The insertions were confirmed, as was co-segregation of the phenotypes with the insertions, by PCR analysis using primers at the *zhd1* (CTCCTGGGGTTTGCAATTGC; GTGTGCATCATGTTCAGCGG) and *zhd21* (TTGTTGCAGCGTGAGACAGG; AGAAATCCATGGAGACTCCGC) loci in combination with Mu-TIR primer (AGAGAAGCCAACGCCAWCGCCTCYATTTCGTC). *Zhd* alleles were backcrossed into the W22 inbred line for at least two generations. Genomic DNA was isolated from leaf tissue using the method described previously (Strable et al., 2017) with slight modification: supernatant of cell lysates was loaded onto 96-well glass fiber filter plates (Pall Laboratory 8032). Gene-specific and transposon multiplex primer PCR was performed under standard conditions with 2X GoTaq Green Master Mix (Promega) with 5% DMSO (v/v).

Tassel and leaf phenotypic data were collected from a population that segregated 1:1:1:1 for the following genotypes: *zhd1-mu2277/+; zhd21-mu8735/+, zhd1-mu2277/zhd1-mu2277; zhd21-mu8735/+, zhd1-mu2277/+; zhd21-mu8735/zhd21-mu8735, zhd1-mu2277/zhd1-mu2277; zhd21-mu8735/zhd21-mu8735*. Phenotypic data were not collected on double mutant plants due to delayed maturation.
The blade/sheath boundary from mature leaves was scanned on each side with an Epson V600 flatbed scanner. Blade angle was quantified from scanned images of leaves with the angle tool and "measure" function in ImageJ. Tassel traits were scored by the following definitions: tassel branch number, the number of basal long branches bearing only spikelet pairs.

ATAC-seq libraries and data analyses
Shoot apices (shoot apex 2) were collected as described above and flash-frozen. Tissue was ground in liquid N and ~ 0.2-0.3 g of tissue was aliquoted into a 15 mL falcon tube. Ground tissue was resuspended in 4 mL of 1x nuclei isolation buffer (16 mM HEPES; pH8, 200 mM sucrose, 0.8 mM MgCl2, 4 mM KCl, 32 % Glycerol, 0.25% Triton X100, 1x complete protease inhibitor, 0.1% 2-ME, 0.1 mM PMSF) very gently at 4°C for 20 minutes and then filtered through 2 sheets of mira cloth. The resulting elutent (~3 mL) was equally split into two 2 mL eppendorf tubes and centrifuged at 1,000 x g for 15 minutes. After discarding the supernatant, nuclei pellets in the two eppendorf tubes were resuspended in 400 µL of 1x tagmentation buffer, combined into a single tube and centrifuged at 1,000 x g for 5 minutes as a wash step (total 2 x washes). The nuclei were resuspended in 100 µL of 1x tagmentation buffer and observed under a microscope (2% acetocarmine stain) to check nuclear integrity. Nuclei were counted using a hemocytometer, and approximately 50,000 nuclei were used for tagmentation. Tagmentation was performed using the Illumina DNA Library Prep Kit (FC-121-1031) and Index Kit (FC-121-1011) with 2.5 µL Tn5 enzyme, 2.5 µL of 2x tagmentation buffer (20 mM Tris Base, 10 mM MgCl2, 20% v/v dimethylformamide), and 20 µL of nuclei for each sample and incubated for 1 hr at 37°C. To each reaction, added 22 µL of H2O, 2.5 µL 10% SDS, and 0.5 µL of Proteinase K and incubated at 55 °C for 1 hr. Tagmented libraries were purified using the Zymo clean and concentrator kit, eluting with resuspension buffer. DNA was quantified using Qubit. 25 ng of tagmented DNA was combined with 2.5 µL of both index primers, 7.5 µL PCR master mix, 2.5 µL NPM and filled to 25 µL with RSB buffer. Libraries were amplified with 11 cycles. Libraries were diluted to 50 µL and cleaned up with a two-sided Ampure XP bead size selection. A 0.5:1 bead:sample ratio followed by a 1.2:1 bead:sample ratio was used to select ~200-1000 bp libraries. Partial lane sequencing was performed using Illumina Novaseq 6000 platform with a paired-end 150 bp reads design. On average for each of the two biological replicates we generated more than 89 million mapped paired-end reads.
For data analysis, raw ATAC-seq reads were trimmed as described for the RNA-seq data with the additional parameters --stringency 1 -q 20. Cleaned reads were mapped to the maize AGPv4 genome using bowtie2 v2.4.5 (Langmead and Salzberg 2012) with default parameters except for --very-sensitive -X 2000 --dovetail. Reads mapped to mitochondria and chloroplast together with PCR duplicates and low mapping quality reads (mapping score < 10) were removed. Peaks were called using MACS2 v2.1.2 (Yong Zhang et al. 2008) with the parameters -f BAMPE --shift -100 --extsize 200 --nomodel -B --SPMR -g 2106338117.

Consensus peaks were generated using the Bioconductor package *GenomicRanges* (Lawrence et al. 2013). BigWig files were generated using bamCoverage with the parameters --binSize 1 --normalizeUsing RPKM.

Data accessibility

Raw and processed data are available through NCBI Gene Expression Omnibus (GEO) database using the identification number GSE180593.

The manuscript utilizes data from various public datasets, including: conserved non-coding sequences (B. Song et al. 2021) and unmethylated regions (Hufford et al. 2021), which were downloaded from https://www.maizegdb.org, tassel inflorescence ATAC-seq and tassel chromatin interaction (Hi-C) (SRA ID: SRR10873334, SRR10873333, SRR10873339, SRR10873340, SRR10873341, SRR10873342, SRR10873343) (Sun et al. 2020), leaf chromatin interaction data (Hi-C) (SRA ID: SRR7889833, SRR7889834) (Ricci et al. 2019).

Acknowledgements

The authors would like to thank members of the Eveland, Lipka and Hake labs who assisted in tissue dissections and/or field phenotyping that contributed to this manuscript, namely Dr. Annis Richardson, Dr. Rajiv Parvathaneni, Dr. Samuel Leiboff, Dr. Matthew Murphy, Dr. Indrajit Kumar, Dr. Samuel Bonfim Fernandes, Ms. Zhonghui Wang, Ms. Adrianna Chepote, Dr. Yuguo Xiao, and Mr. Jake Sinkowitz. Also, a dear thanks to Dr. Todd Mockler and members of his team, Mr. Robert Lowery, Mr. Darren O'Brian, and Dr. Phil Ozersky, for their assistance in field phenotyping.

We also thank Dr. Baoxing Song and Dr. M.Cinta Romay for providing the AGPv4 genome alignment BAM files for the resequencing data of the Maize 282 Association Panel.

A special thank you to Kevin Reilly and his team in the Danforth Center Integrated Plant Growth Facility for their help with plant care as well as Noah Fahlgren and his team in the Danforth Data Science Core Facility with maintaining computational infrastructure used for this project.

This work was funded by a National Science Foundation Plant Genome Research Project award # IOS-1733606 to ALE, AEL and SH.

Authors' contributions

ALE, AEL and SH designed the research. EB performed network analyses, data integration and interpretation. BRR performed genotype selection and multi-trait GWAS. MB and JY contributed to experimental design and performed molecular and genetics experiments. JS performed genetic analyses of *zhds*, EB and ALE wrote the paper with input from all authors. All authors contributed to editing the final manuscript, read and approved the final manuscript.

References

Abraham-Juárez, María Jazmín, Allison C. Barnes, Alejandro Aragón-Raygoza, Destiny Tyson, Andi Kur, Josh Strable, and Rubén Rellán-Álvarez. 2021. "The Arches and Spandrels of Maize Domestication, Adaptation, and Improvement." *Current Opinion in Plant Biology* 64 (December): 102124. https://doi.org/10.1016/j.pbi.2021.102124.

Alon, Uri. 2007. "Network Motifs: Theory and Experimental Approaches." *Nature Reviews. Genetics* 8 (6): 450–61. https://doi.org/10.1038/nrg2102.

Bai, Fang, Renata Reinheimer, Diego Durantini, Elizabeth A. Kellogg, and Robert J. Schmidt. 2012. "TCP Transcription Factor, BRANCH ANGLE DEFECTIVE 1 (BAD1), Is Required for Normal Tassel Branch Angle Formation in Maize." *Proceedings of the National Academy of Sciences of the United States of America* 109 (30): 12225–30. https://doi.org/10.1073/pnas.1202439109.

Bailey-Serres, Julia, Jane E. Parker, Elizabeth A. Ainsworth, Giles E. D. Oldroyd, and Julian I. Schroeder. 2019. "Genetic Strategies for Improving Crop Yields." *Nature* 575 (7781): 109–18. https://doi.org/10.1038/s41586-019-1679-0.

Becraft, P. W., D. K. Bongard-Pierce, A. W. Sylvester, R. S. Poethig, and M. Freeling. 1990. "The Liguleless-1 Gene Acts Tissue Specifically in Maize Leaf Development." *Developmental Biology* 141 (1): 220–32. https://www.ncbi.nlm.nih.gov/pubmed/2391003.

Bell, Elizabeth M., Wan-Ching Lin, Aman Y. Husbands, Lifeng Yu, Venkateswari Jaganatha, Barbara Jablonska, Amanda Mangeon, Michael M. Neff, Thomas Girke, and Patricia S. Springer. 2012. "Arabidopsis Lateral Organ Boundaries Negatively Regulates Brassinosteroid Accumulation to Limit Growth in Organ Boundaries." *Proceedings of the National Academy of Sciences of the United States of America* 109 (51): 21146–51. https://doi.org/10.1073/pnas.1210789109.

Benjamini, Yoav, and Yosef Hochberg. 1995. "Controlling the False Discovery Rate: A Practical and Powerful Approach to Multiple Testing." *Journal of the Royal Statistical Society: Series B (Methodological)*. https://doi.org/10.1111/j.2517-6161.1995.tb02031.x.

Bolduc, Nathalie, and Sarah Hake. 2009. "The Maize Transcription Factor KNOTTED1 Directly Regulates the Gibberellin Catabolism Gene ga2ox1." *The Plant Cell* 21 (6): 1647–58. https://doi.org/10.1105/tpc.109.068221.

Bolduc, Nathalie, Alper Yilmaz, Maria Katherine Mejia-Guerra, Kengo Morohashi, Devin O'Connor, Erich Grotewold, and Sarah Hake. 2012. "Unraveling the KNOTTED1 Regulatory Network in Maize Meristems." *Genes & Development* 26 (15): 1685–90. https://doi.org/10.1101/gad.193433.112.

Bortiri, Esteban, George Chuck, Erik Vollbrecht, Torbert Rocheford, Rob Martienssen, and Sarah Hake. 2006. "ramosa2 Encodes a LATERAL ORGAN BOUNDARY Domain Protein That Determines the Fate of Stem Cells in Branch Meristems of Maize." *The Plant Cell* 18 (3): 574–85. https://doi.org/10.1105/tpc.105.039032.

Bouchet, Sophie, Marcus O. Olatoye, Sandeep R. Marla, Ramasamy Perumal, Tesfaye Tesso, Jianming Yu, Mitch Tuinstra, and Geoffrey P. Morris. 2017. "Increased Power To Dissect Adaptive Traits in Global Sorghum Diversity Using a Nested Association Mapping Population." *Genetics* 206 (2): 573–85. https://doi.org/10.1534/genetics.116.198499.

Brown, Patrick J., Narasimham Upadyayula, Gregory S. Mahone, Feng Tian, Peter J. Bradbury, Sean Myles, James B. Holland, et al. 2011. "Distinct Genetic Architectures for Male and Female Inflorescence Traits of Maize." *PLoS Genetics* 7 (11): e1002383. https://doi.org/10.1371/journal.pgen.1002383.

Burdo, Brett, John Gray, Mary P. Goetting-Minesky, Bettina Wittler, Matthew Hunt, Tai Li, David Velliquette, et al. 2014. "The Maize TFome--Development of a Transcription Factor Open Reading Frame Collection for Functional Genomics." *The Plant Journal: For Cell and Molecular Biology* 80 (2): 356–66. https://doi.org/10.1111/tpj.12623.

Butler, D. G., B. R. Cullis, A. R. Gilmour, B. J. Gogel, and R. Thompson. 2017. “ASReml-R Reference Manual Version 4.” VSN International Ltd, Hemel Hempstead, HP1 1ES, UK.
Carroll, Sean B. 2005. “Evolution at Two Levels: On Genes and Form.” *PLoS Biology* 3 (7): e245. https://doi.org/10.1371/journal.pbio.0030245.
Carroll, Sean B. 2008. “Evo-Devo and an Expanding Evolutionary Synthesis: A Genetic Theory of Morphological Evolution.” *Cell* 134 (1): 25–36. https://doi.org/10.1016/j.cell.2008.06.030.
Casa, Alexandra M., Gael Pressoir, Patrick J. Brown, Sharon E. Mitchell, William L. Rooney, Mitchell R. Tuinstra, Cleve D. Franks, and Stephen Kresovich. 2008. “Community Resources and Strategies for Association Mapping in Sorghum.” *Crop Science* 48 (1): 30–40. https://doi.org/10.2135/cropsci2007.02.0080.
Chang, Christopher C., Carson C. Chow, Laurent Cam Tellier, Shashaank Vattikuti, Shaun M. Purcell, and James J. Lee. 2015. “Second-Generation PLINK: Rising to the Challenge of Larger and Richer Datasets.” *GigaScience*. https://doi.org/10.1186/s13742-015-0047-8.
Chen, Angela H., and Alexander E. Lipka. 2016. “The Use of Targeted Marker Subsets to Account for Population Structure and Relatedness in Genome-Wide Association Studies of Maize (Zea Mays L.).” *G3* 6 (8): 2365–74. https://doi.org/10.1534/g3.116.029090.
Csardi, Gabor, and Tamas Nepusz. 2006. “The Igraph Software Package for Complex Network Research.” *InterJournal Complex Systems* 1695: 1695.
Danecek, Petr, Adam Auton, Goncalo Abecasis, Cornelis A. Albers, Eric Banks, Mark A. DePristo, Robert E. Handsaker, et al. 2011. “The Variant Call Format and VCFtools.” *Bioinformatics* 27 (15): 2156–58. https://doi.org/10.1093/bioinformatics/btr330.
Doebley, J., and L. Lukens. 1998. “Transcriptional Regulators and the Evolution of Plant Form.” *The Plant Cell* 10 (7): 1075–82. https://doi.org/10.1105/tpc.10.7.1075.
Doebley, John F., Brandon S. Gaut, and Bruce D. Smith. 2006. “The Molecular Genetics of Crop Domestication.” *Cell* 127 (7): 1309–21. https://doi.org/10.1016/j.cell.2006.12.006.
Duncan, William G., William A. Williams, and Robert S. Loomis. 1967. “Tassels and the Productivity of Maize 1.” *Crop Science* 7 (1): 37–39. https://doi.org/10.2135/cropsci1967.0011183x000700010013x.
Duvick, D. N. 2005. “GENETIC PROGRESS IN YIELD OF UNITED STATES MAIZE (Zea Mays L.).” *Maydica* 50: 193–202.
Eilers, Paul H. C., and Brian D. Marx. 1996. “Flexible Smoothing with B-Splines and Penalties.” *Schweizerische Monatsschrift Fur Zahnheilkunde = Revue Mensuelle Suisse D’odonto-Stomatologie / SSO* 11 (2): 89–121. https://doi.org/10.1214/ss/1038425655.
Eshed, Yuval, and Zachary B. Lippman. 2019. “Revolutions in Agriculture Chart a Course for Targeted Breeding of Old and New Crops.” *Science* 366 (6466). https://doi.org/10.1126/science.aax0025.
Eveland, Andrea L., Alexander Goldshmidt, Michael Pautler, Kengo Morohashi, Christophe Liseron-Monfils, Michael W. Lewis, Sunita Kumari, et al. 2014. “Regulatory Modules Controlling Maize Inflorescence Architecture.” *Genome Research* 24 (3): 431–43. https://doi.org/10.1101/gr.166397.113.
Flint-Garcia, Sherry A., Anne-Céline Thuillet, Jianming Yu, Gael Pressoir, Susan M. Romero, Sharon E. Mitchell, John Doebley, Stephen Kresovich, Major M. Goodman, and Edward S. Buckler. 2005. “Maize Association Population: A High-Resolution Platform for Quantitative Trait Locus Dissection.” *The Plant Journal: For Cell and Molecular Biology* 44 (6): 1054–64. https://doi.org/10.1111/j.1365-313X.2005.02591.x.
Gaarslev, Natalia, Gwen Swinnen, and Sebastian Soyk. 2021. “Meristem Transitions and Plant Architecture—learning from Domestication for Crop Breeding.” *Plant Physiology* 187 (3): 1045–56. https://doi.org/10.1093/plphys/kiab388.
Gendron, Joshua M., Jiang-Shu Liu, Min Fan, Ming-Yi Bai, Stephan Wenkel, Patricia S. Springer, M. Kathryn Barton, and Zhi-Yong Wang. 2012. “Brassinosteroids Regulate Organ Boundary Formation in the Shoot Apical Meristem of Arabidopsis.” *Proceedings of the*

National Academy of Sciences of the United States of America 109 (51): 21152–57. https://doi.org/10.1073/pnas.1210799110.
Gilmour, Arthur R., Robin Thompson, and Brian R. Cullis. 1995. “Average Information REML: An Efficient Algorithm for Variance Parameter Estimation in Linear Mixed Models.” *Biometrics* 51 (4): 1440–50. https://doi.org/10.2307/2533274.
Grassini, Patricio, Kent M. Eskridge, and Kenneth G. Cassman. 2013. “Distinguishing between Yield Advances and Yield Plateaus in Historical Crop Production Trends.” *Nature Communications* 4: 2918. https://doi.org/10.1038/ncomms3918.
Harper, L., and M. Freeling. 1996. “Interactions of liguleless1 and liguleless2 Function during Ligule Induction in Maize.” *Genetics* 144 (4): 1871–82. https://www.ncbi.nlm.nih.gov/pubmed/8978070.
Hendelman, Anat, Sophia Zebell, Daniel Rodriguez-Leal, Noah Dukler, Gina Robitaille, Xuelin Wu, Jamie Kostyun, et al. 2021. “Conserved Pleiotropy of an Ancient Plant Homeobox Gene Uncovered by Cis-Regulatory Dissection.” *Cell* 184 (7): 1724–39.e16. https://doi.org/10.1016/j.cell.2021.02.001.
Huang, Meng, Xiaolei Liu, Yao Zhou, Ryan M. Summers, and Zhiwu Zhang. 2019. “BLINK: A Package for the next Level of Genome-Wide Association Studies with Both Individuals and Markers in the Millions.” *GigaScience*. https://doi.org/10.1093/gigascience/giy154.
Hufford, Matthew B., Arun S. Seetharam, Margaret R. Woodhouse, Kapeel M. Chougule, Shujun Ou, Jianing Liu, William A. Ricci, et al. 2021. “De Novo Assembly, Annotation, and Comparative Analysis of 26 Diverse Maize Genomes.” *Science* 373 (6555): 655–62. https://doi.org/10.1126/science.abg5289.
Huynh-Thu, Vân Anh, Alexandre Irrthum, Louis Wehenkel, and Pierre Geurts. 2010. “Inferring Regulatory Networks from Expression Data Using Tree-Based Methods.” *PloS One* 5 (9). https://doi.org/10.1371/journal.pone.0012776.
Jiao, Yinping, Paul Peluso, Jinghua Shi, Tiffany Liang, Michelle C. Stitzer, Bo Wang, Michael S. Campbell, et al. 2017. “Improved Maize Reference Genome with Single-Molecule Technologies.” *Nature*, June. https://doi.org/10.1038/nature22971.
Johnston, Robyn, Minghui Wang, Qi Sun, Anne W. Sylvester, Sarah Hake, and Michael J. Scanlon. 2014. “Transcriptomic Analyses Indicate That Maize Ligule Development Recapitulates Gene Expression Patterns That Occur during Lateral Organ Initiation.” *The Plant Cell* 26 (12): 4718–32. https://doi.org/10.1105/tpc.114.132688.
Kellogg, Elizabeth A. 2007. “Floral Displays: Genetic Control of Grass Inflorescences.” *Current Opinion in Plant Biology* 10 (1): 26–31. https://doi.org/10.1016/j.pbi.2006.11.009.
Kir, Gokhan. 2015. “Regulation of Shoot Development in Maize via Brassinosteroid Signaling.” Iowa State University. https://doi.org/10.31274/etd-180810-3931.
Kir, Gokhan, Huaxun Ye, Hilde Nelissen, Anjanasree K. Neelakandan, Andree S. Kusnandar, Anding Luo, Dirk Inzé, Anne W. Sylvester, Yanhai Yin, and Philip W. Becraft. 2015. “RNA Interference Knockdown of BRASSINOSTEROID INSENSITIVE1 in Maize Reveals Novel Functions for Brassinosteroid Signaling in Controlling Plant Architecture.” *Plant Physiology* 169 (1): 826–39. https://doi.org/10.1104/pp.15.00367.
Langfelder, Peter, and Steve Horvath. 2007. “Eigengene Networks for Studying the Relationships between Co-Expression Modules.” *BMC Systems Biology* 1 (November): 54. https://doi.org/10.1186/1752-0509-1-54.
Langfelder, Peter, and Steve Horvath. 2008. “WGCNA: An R Package for Weighted Correlation Network Analysis.” *BMC Bioinformatics* 9 (December): 559. https://doi.org/10.1186/1471-2105-9-559.
Langmead, Ben, and Steven L. Salzberg. 2012. “Fast Gapped-Read Alignment with Bowtie 2.” *Nature Methods* 9 (4): 357–59. https://doi.org/10.1038/nmeth.1923.
Lawrence, Michael, Wolfgang Huber, Hervé Pages, Patrick Aboyoun, Marc Carlson, Robert Gentleman, Martin T. Morgan, and Vincent J. Carey. 2013. “Software for Computing and

Annotating Genomic Ranges." *PLoS Computational Biology* 9 (8): e1003118. https://doi.org/10.1371/journal.pcbi.1003118.
Lee, Sang Hong, and Julius H. J. van der Werf. 2006. "An Efficient Variance Component Approach Implementing an Average Information REML Suitable for Combined LD and Linkage Mapping with a General Complex Pedigree." *Genetics, Selection, Evolution: GSE* 38 (1): 25–43. https://doi.org/10.1186/1297-9686-38-1-25.
Leiboff, Samuel, Josh Strable, Robyn Johnston, Silvia Federici, Anne W. Sylvester, and Michael J. Scanlon. 2020. "Network Analyses Identify a Transcriptomic Proximodistal Prepattern in the Maize Leaf Primordium." *The New Phytologist*, December. https://doi.org/10.1111/nph.17132.
Lewis, Michael W., Nathalie Bolduc, Kayley Hake, Yadanar Htike, Angela Hay, Héctor Candela, and Sarah Hake. 2014. "Gene Regulatory Interactions at Lateral Organ Boundaries in Maize." *Development* 141 (23): 4590–97. https://doi.org/10.1242/dev.111955.
Lipka, Alexander E., Michael A. Gore, Maria Magallanes-Lundback, Alex Mesberg, Haining Lin, Tyler Tiede, Charles Chen, et al. 2013. "Genome-Wide Association Study and Pathway-Level Analysis of Tocochromanol Levels in Maize Grain." *G3* 3 (8): 1287–99. https://doi.org/10.1534/g3.113.006148.
Lipka, Alexander E., Feng Tian, Qishan Wang, Jason Peiffer, Meng Li, Peter J. Bradbury, Michael A. Gore, Edward S. Buckler, and Zhiwu Zhang. 2012. "GAPIT: Genome Association and Prediction Integrated Tool." *Bioinformatics* 28 (18): 2397–99. https://doi.org/10.1093/bioinformatics/bts444.
Liu, Wen-Yu, Hsin-Hung Lin, Chun-Ping Yu, Chao-Kang Chang, Hsiang-June Chen, Jinn-Jy Lin, Mei-Yeh Jade Lu, et al. 2020. "Maize ANT1 Modulates Vascular Development, Chloroplast Development, Photosynthesis, and Plant Growth." *Proceedings of the National Academy of Sciences of the United States of America* 117 (35): 21747–56. https://doi.org/10.1073/pnas.2012245117.
Love, Michael I., Wolfgang Huber, and Simon Anders. 2014. "Moderated Estimation of Fold Change and Dispersion for RNA-Seq Data with DESeq2." *Genome Biology* 15 (12): 550. https://doi.org/10.1186/s13059-014-0550-8.
Mantilla Perez, Maria B., Jing Zhao, Yanhai Yin, Jieyun Hu, and Maria G. Salas Fernandez. 2014. "Association Mapping of Brassinosteroid Candidate Genes and Plant Architecture in a Diverse Panel of Sorghum Bicolor." *TAG. Theoretical and Applied Genetics. Theoretische Und Angewandte Genetik* 127 (12): 2645–62. https://doi.org/10.1007/s00122-014-2405-9.
Marand, Alexandre P., Andrea L. Eveland, Kerstin Kaufmann, and Nathan M. Springer. 2023. "Cis-Regulatory Elements in Plant Development, Adaptation, and Evolution." *Annual Review of Plant Biology* 74 (May): 111–37. https://doi.org/10.1146/annurev-arplant-070122-030236.
Martin, Marcel. 2011. "Cutadapt Removes Adapter Sequences from High-Throughput Sequencing Reads." *EMBnet.journal* 17 (1): 10–12. https://doi.org/10.14806/ej.17.1.200.
McCarty, Donald R., Andrew Mark Settles, Masaharu Suzuki, Bao Cai Tan, Susan Latshaw, Tim Porch, Kevin Robin, et al. 2005. "Steady-State Transposon Mutagenesis in Inbred Maize." *The Plant Journal: For Cell and Molecular Biology* 44 (1): 52–61. https://onlinelibrary.wiley.com/doi/abs/10.1111/j.1365-313X.2005.02509.x.
McSteen, Paula, Simon Malcomber, Andrea Skirpan, China Lunde, Xianting Wu, Elizabeth Kellogg, and Sarah Hake. 2007. "Barren inflorescence2 Encodes a Co-Ortholog of the PINOID Serine/threonine Kinase and Is Required for Organogenesis during Inflorescence and Vegetative Development in Maize." *Plant Physiology* 144 (2): 1000–1011. https://doi.org/10.1104/pp.107.098558.
Milo, R., S. Shen-Orr, S. Itzkovitz, N. Kashtan, D. Chklovskii, and U. Alon. 2002. "Network Motifs: Simple Building Blocks of Complex Networks." *Science* 298 (5594): 824–27. https://doi.org/10.1126/science.298.5594.824.

Money, Daniel, Kyle Gardner, Zoë Migicovsky, Heidi Schwaninger, Gan-Yuan Zhong, and Sean Myles. 2015. “LinkImpute: Fast and Accurate Genotype Imputation for Nonmodel Organisms.” *G3* 5 (11): 2383–90. https://doi.org/10.1534/g3.115.021667.

Moreno, M. A., L. C. Harper, R. W. Krueger, S. L. Dellaporta, and M. Freeling. 1997. “liguleless1 Encodes a Nuclear-Localized Protein Required for Induction of Ligules and Auricles during Maize Leaf Organogenesis.” *Genes & Development* 11 (5): 616–28. https://doi.org/10.1101/gad.11.5.616.

Morris, Geoffrey P., Punna Ramu, Santosh P. Deshpande, C. Thomas Hash, Trushar Shah, Hari D. Upadhyaya, Oscar Riera-Lizarazu, et al. 2013. “Population Genomic and Genome-Wide Association Studies of Agroclimatic Traits in Sorghum.” *Proceedings of the National Academy of Sciences of the United States of America* 110 (2): 453–58. https://doi.org/10.1073/pnas.1215985110.

Nei, M., and W. H. Li. 1979. “Mathematical Model for Studying Genetic Variation in Terms of Restriction Endonucleases.” *Proceedings of the National Academy of Sciences of the United States of America* 76 (10): 5269–73. https://doi.org/10.1073/pnas.76.10.5269.

Parvathaneni, Rajiv K., Edoardo Bertolini, Md Shamimuzzaman, Daniel L. Vera, Pei-Yau Lung, Brian R. Rice, Jinfeng Zhang, et al. 2020. “The Regulatory Landscape of Early Maize Inflorescence Development.” *Genome Biology* 21 (1): 165. https://doi.org/10.1186/s13059-020-02070-8.

Peiffer, Jason A., Maria C. Romay, Michael A. Gore, Sherry A. Flint-Garcia, Zhiwu Zhang, Mark J. Millard, Candice A. C. Gardner, et al. 2014. “The Genetic Architecture of Maize Height.” *Genetics* 196 (4): 1337–56. https://doi.org/10.1534/genetics.113.159152.

Ricci, William A., Zefu Lu, Lexiang Ji, Alexandre P. Marand, Christina L. Ethridge, Nathalie G. Murphy, Jaclyn M. Noshay, et al. 2019. “Widespread Long-Range Cis-Regulatory Elements in the Maize Genome.” *Nature Plants*, November. https://doi.org/10.1038/s41477-019-0547-0.

Rice, Brian R., Samuel B. Fernandes, and Alexander E. Lipka. 2020. “Multi-Trait Genome-Wide Association Studies Reveal Loci Associated with Maize Inflorescence and Leaf Architecture.” *Plant & Cell Physiology* 61 (8): 1427–37. https://doi.org/10.1093/pcp/pcaa039.

Richardson, Annis E., and Sarah Hake. 2018. “Drawing a Line: Grasses and Boundaries.” *Plants* 8 (1). https://doi.org/10.3390/plants8010004.

Romay, Maria C., Mark J. Millard, Jeffrey C. Glaubitz, Jason A. Peiffer, Kelly L. Swarts, Terry M. Casstevens, Robert J. Elshire, et al. 2013. “Comprehensive Genotyping of the USA National Maize Inbred Seed Bank.” *Genome Biology* 14 (6): R55. https://doi.org/10.1186/gb-2013-14-6-r55.

Schwarz, Gideon. 1978. “Estimating the Dimension of a Model.” *The Annals of Statistics* 6 (2): 461–64. https://doi.org/10.1214/aos/1176344136.

Soneson, Charlotte, Michael I. Love, and Mark D. Robinson. 2015. “Differential Analyses for RNA-Seq: Transcript-Level Estimates Improve Gene-Level Inferences.” *F1000Research* 4 (December): 1521. https://doi.org/10.12688/f1000research.7563.2.

Song, Baoxing, Edward S. Buckler, Hai Wang, Yaoyao Wu, Evan Rees, Elizabeth A. Kellogg, Daniel J. Gates, et al. 2021. “Conserved Noncoding Sequences Provide Insights into Regulatory Sequence and Loss of Gene Expression in Maize.” *Genome Research* 31 (7): 1245–57. https://doi.org/10.1101/gr.266528.120.

Song, Xiaoguang, Xiangbing Meng, Hongyan Guo, Qiao Cheng, Yanhui Jing, Mingjiang Chen, Guifu Liu, et al. 2022. “Targeting a Gene Regulatory Element Enhances Rice Grain Yield by Decoupling Panicle Number and Size.” *Nature Biotechnology*, April. https://doi.org/10.1038/s41587-022-01281-7.

Speed, Doug, Na Cai, UCLEB Consortium, Michael R. Johnson, Sergey Nejentsev, and David J. Balding. 2017. “Reevaluation of SNP Heritability in Complex Human Traits.” *Nature*

Genetics 49 (7): 986–92. https://doi.org/10.1038/ng.3865.
Srivastava, Avi, Laraib Malik, Hirak Sarkar, Mohsen Zakeri, Fatemeh Almodaresi, Charlotte Soneson, Michael I. Love, Carl Kingsford, and Rob Patro. 2020. "Alignment and Mapping Methodology Influence Transcript Abundance Estimation." *Genome Biology* 21 (1): 239. https://doi.org/10.1186/s13059-020-02151-8.
Sun, Yonghao, Liang Dong, Ying Zhang, Da Lin, Weize Xu, Changxiong Ke, Linqian Han, et al. 2020. "3D Genome Architecture Coordinates Trans and Cis Regulation of Differentially Expressed Ear and Tassel Genes in Maize." *Genome Biology* 21 (1): 143. https://doi.org/10.1186/s13059-020-02063-7.
Tian, Feng, Peter J. Bradbury, Patrick J. Brown, Hsiaoyi Hung, Qi Sun, Sherry Flint-Garcia, Torbert R. Rocheford, Michael D. McMullen, James B. Holland, and Edward S. Buckler. 2011. "Genome-Wide Association Study of Leaf Architecture in the Maize Nested Association Mapping Population." *Nature Genetics* 43 (2): 159–62. https://doi.org/10.1038/ng.746.
Tian, Jinge, Chenglong Wang, Jinliang Xia, Lishuan Wu, Guanghui Xu, Weihao Wu, Dan Li, et al. 2019. "Teosinte Ligule Allele Narrows Plant Architecture and Enhances High-Density Maize Yields." *Science* 365 (6454): 658–64. https://doi.org/10.1126/science.aax5482.
Vajk, Angus Hugo. 2019. "The Role of FUN in Sexual Differentiation and Leaf Development in Zea Mays." UC Berkeley. https://escholarship.org/uc/item/29r2x7hh.
VanRaden, P. M. 2008. "Efficient Methods to Compute Genomic Predictions." *Journal of Dairy Science* 91 (11): 4414–23. https://doi.org/10.3168/jds.2007-0980.
Vollbrecht, Erik, Patricia S. Springer, Lindee Goh, Edward S. Buckler 4th, and Robert Martienssen. 2005. "Architecture of Floral Branch Systems in Maize and Related Grasses." *Nature* 436 (7054): 1119–26. https://doi.org/10.1038/nature03892.
Vollbrecht, E., B. Veit, N. Sinha, and S. Hake. 1991. "The Developmental Gene Knotted-1 Is a Member of a Maize Homeobox Gene Family." *Nature* 350 (6315): 241–43. https://doi.org/10.1038/350241a0.
Walsh, J., and M. Freeling. 1999. "The liguleless2 Gene of Maize Functions during the Transition from the Vegetative to the Reproductive Shoot Apex." *The Plant Journal: For Cell and Molecular Biology* 19 (4): 489–95. https://doi.org/10.1046/j.1365-313X.1999.00541.x.
Walsh, J., C. A. Waters, and M. Freeling. 1998. "The Maize Gene liguleless2 Encodes a Basic Leucine Zipper Protein Involved in the Establishment of the Leaf Blade-Sheath Boundary." *Genes & Development* 12 (2): 208–18. https://www.ncbi.nlm.nih.gov/pubmed/9490265.
Wang, Baobao, Zechuan Lin, Xin Li, Yongping Zhao, Binbin Zhao, Guangxia Wu, Xiaojing Ma, et al. 2020. "Genome-Wide Selection and Genetic Improvement during Modern Maize Breeding." *Nature Genetics* 52 (6): 565–71. https://doi.org/10.1038/s41588-020-0616-3.
Wang, Huai, Anthony J. Studer, Qiong Zhao, Robert Meeley, and John F. Doebley. 2015. "Evidence That the Origin of Naked Kernels During Maize Domestication Was Caused by a Single Amino Acid Substitution in tga1." *Genetics* 200 (3): 965–74. https://doi.org/10.1534/genetics.115.175752.
Whipple, Clinton J. 2017. "Grass Inflorescence Architecture and Evolution: The Origin of Novel Signaling Centers." *The New Phytologist* 216 (2): 367–72. https://doi.org/10.1111/nph.14538.
Wimalanathan, Kokulapalan, and Carolyn J. Lawrence-Dill. 2021. "Gene Ontology Meta Annotator for Plants (GOMAP)." *Plant Methods* 17 (1): 54. https://doi.org/10.1186/s13007-021-00754-1.
Wittkopp, Patricia J., and Gizem Kalay. 2011. "Cis-Regulatory Elements: Molecular Mechanisms and Evolutionary Processes Underlying Divergence." *Nature Reviews. Genetics* 13 (1): 59–69. https://doi.org/10.1038/nrg3095.
Xiao, Yuguo, Jinyan Guo, Zhaobin Dong, Annis Richardson, Erin Patterson, Sidney Mangrum, Seth Bybee, et al. 2022. "Boundary Domain Genes Were Recruited to Suppress Bract

Growth and Promote Branching in Maize." *Science Advances* 8 (24): eabm6835. https://doi.org/10.1126/sciadv.abm6835.

Yu, Guangchuang, Li-Gen Wang, Yanyan Han, and Qing-Yu He. 2012. "clusterProfiler: An R Package for Comparing Biological Themes among Gene Clusters." *Omics: A Journal of Integrative Biology* 16 (5): 284–87. https://doi.org/10.1089/omi.2011.0118.

Zhang, Yang, Daniel W. Ngu, Daniel Carvalho, Zhikai Liang, Yumou Qiu, Rebecca L. Roston, and James C. Schnable. 2017. "Differentially Regulated Orthologs in Sorghum and the Subgenomes of Maize." *The Plant Cell* 29 (8): 1938–51. https://doi.org/10.1105/tpc.17.00354.

Zhang, Yong, Tao Liu, Clifford A. Meyer, Jérôme Eeckhoute, David S. Johnson, Bradley E. Bernstein, Chad Nusbaum, et al. 2008. "Model-Based Analysis of ChIP-Seq (MACS)." *Genome Biology* 9 (9): R137. https://doi.org/10.1186/gb-2008-9-9-r137.

Zhao, Hao, Zhifu Sun, Jing Wang, Haojie Huang, Jean-Pierre Kocher, and Liguo Wang. 2014. "CrossMap: A Versatile Tool for Coordinate Conversion between Genome Assemblies." *Bioinformatics* 30 (7): 1006–7. https://doi.org/10.1093/bioinformatics/btt730.

Zhou, Xiang, and Matthew Stephens. 2014. "Efficient Multivariate Linear Mixed Model Algorithms for Genome-Wide Association Studies." *Nature Methods* 11 (4): 407–9. https://doi.org/10.1038/nmeth.2848.

Figure Legends

Fig. 1: Transcriptional analyses across maize mutants with defects in leaf angle and tassel branching.

a) Panel of maize mutants used in this study depicting unique tassel branching phenotypes compared to B73 controls. Color scale in the heatmap below indicates severity of tassel branch number (TBN), tassel branch angle (TBA) and leaf angle (LA) phenotype deviations from B73 controls; dark blue-to-white is strong-to-weak phenotype. **b)** Enrichment of GO terms associated with differentially expressed (DE) gene sets identified during the shift from stage 1 to stage 2 tassels and from shoot apex 1 to shoot apex 2. **c)** A 2-dimensional section of the first and second PC from the normal B73 tassel developmental gradient (n = 20). The blue line represents the b-spline fit with three degrees of freedom modeled within the dataset and used to classify samples relative to their developmental progression coded as expression time (ET). Squared dots represent the 20 tassel samples in ET. The underlying dot plot represents stages 1 and 2 tassel primordia from the different mutant backgrounds. Mutant data points are color-coded relative to B73 ET. The black arrow represents stages of meristem development along normal tassel developmental time: inflorescence meristem (IM), branch meristem (BM), spikelet pair meristem (SPM), spikelet meristem (SM). **d)** Venn diagram shows genes that are DE between tassel primordia at stage 1 and 2 in *bri1-RNAi* and *bin2-RNAi* mutants compared to B73 controls. Those with higher variation in expression at stg1 are shown in parentheses. The ternary plot below shows the relative expression of genes commonly mis-expressed between the two mutants compared to B73 at stage 1. Each dot represents a gene and its coordinates indicate relative expression in the three genotypes. Some examples of classical maize genes are noted. **e)** The top heatmap shows GO terms enriched among DE gene sets commonly expressed either higher or lower in the BR mutants compared to B73 controls in stage 1 tassels (from the ternary plot in d); the bottom heatmap shows overrepresented TF classes among genes expressed higher in *bri1* and *bin2* mutants at stage 1 and those expressed higher in *bin2* only compared to B73 controls. **f)** Relative gene expression trends are shown for ZHD and SBP TF family members that were expressed higher in *bin2* and/or *bri1* mutants compared to B73 controls at stage 1.

Fig. 2: Conserved and divergent network connections between tassel and leaf gene regulatory networks.

a) Gene co-expression network (GCN) preservation between 'tassel' and 'leaf' networks. Preserved modules are indicated by color and connected by lines (width is proportional to number of preserved genes). Colored boxes beneath the plot represent selected (starred) preserved gene regulatory sub-modules. Number of nodes in each preserved sub-module is indicated. **b)** Topological graph representation of preserved TFs in the 'tassel'-'leaf' "brown-green" sub-module based on data from GCN (edge weight) and gene regulatory network (GRN; edge directionality). Pink edges represent preserved regulatory connections and brown or green edges represent the network-specific wires. **c)** Topological graph representation of closest TF neighbors to *liguleless2* (*lg2*) in the 'tassel' and 'leaf' networks based on data from GCN (edge weight) and GRN (edge directionality). Pink edges represent preserved connections and blue or brown/green edges represent network-specific wires. The edge length is proportional to the

weight of gene co-expression. Maize gene labels are from MaizeGDB or AGPv4 as Zm00001d$_{(6)}$.

Fig. 3: Analysis of three-node network motifs.
a) The number and type of three-node motifs identified in 'tassel' and 'leaf' networks compared to randomized networks (n = 1,000). The x-axis represents the motif type (from A to J) of three-node motifs with edge number ≥ 3. **b)** Top 100 ranked TFs based on their occurrence in the three-node motifs grouped by family. Bars represent TF frequency in the three-node motif (scale in red is TF frequency / 10,000); non-normalized values are between brackets. TF labels are from MaizeGDB or AGPv4 as Zm00001d$_{(6)}$. **c)** Examples of feed-forward loop (FFL) motifs mediated by select TFs. The heatmap displays overrepresented TFs in FFL$_{(X)}$, (examples of genes in each TF family are noted). Nodes represent genes, while the directed edges represent the potential regulatory relationships.

Fig. 4: Multi-trait GWAS detected candidate pleiotropic genes for LA and TBN.
a) Phenotypic Principal Components (PhPCs) of Leaf Angle (LA) and Tassel Branch Number (TBN). Individuals are plotted according to their PhPC1 scores of LA and TBN on the x-axis and their PhPC2 scores on the y-axis. The percentage of total variance explained by a component is listed in parentheses on the axis. Blue arrows represent trait loadings for a given PhPC where its direction on the x-axis represents its contribution to PhPC1 and direction on the y-axis, its contribution to PhPC2. Subpopulations are color-coded and grouped according to PhPCs. **b)** Analysis of module-trait relationships for the combined gene co-expression network. Modules are represented as colored boxes with the number of co-expressed genes indicated. The correlogram to the right represents the module trait relationship where shades of blue and red represent positive and negative Pearson's correlation, respectively, with darker color indicating a stronger positive or negative correlation. Modules representing more than 80% of the whole genome heritability (h^2) for TBN and LA are indicated. **c)** Multi-trait GWAS results using subsets of markers within 2 kb proximity of genes in the six co-expression modules with significant h^2 in panel b (top) and in the top 200 interconnected TFs within three-node motifs from Fig. 3b. Brown and blue dots represent significant SNP-trait associations; blue dots indicate loci identified in both analyses. **d)** Topological graph representation of a sub-network including *ereb184*, *zhd21* and their predicted downstream target genes based on data from the 'leaf' GRN (edge directionality).

Fig. 5: GWAS for LA in sorghum using biological information derived from maize.
a) LA narrow-sense heritability of 158 sorghum-maize syntenic orthologs in comparison to a null distribution (violin plot). Purple line represents 95% cut-off, orange line represents LA h^2 of the sorghum orthologs, green line is the whole genome LA h^2. **b)** Manhattan plot showing GWAS results for LA based on markers in proximity of the 158 sorghum-maize syntenic orthologs. Purple dots represent significant SNP-trait associations for LA. **c)** Topological graph representation of *ereb114* and its closest network neighbors in the maize 'leaf' GCN (edge weight) and GRN (edge directionality). Green and purple nodes and edges are colored based on module assignment in the 'leaf' GCN. Pink edges represent preserved connections with the 'tassel' GCN. Edge length is proportional with the gene co-expression weight.

Fig. 6: Characterization of pleiotropic phenotypes from combining *zhd* mutant alleles.
a) Representative tassel branch and leaf angle phenotypes resulting from genetic interactions between mutant alleles of *zhd1* and *zhd21*, from left to right: *zhd1/+;zhd21/+*, *zhd1/+;zhd21/zhd21*, *zhd1/1;zhd21/+*. Black bar = 1cm. **b)** Among combinations of mutant alleles, *zhd1/1;zhd21/+* showed significant differences in TBN and LA from the *zhd1/+*;*zhd21/+* normal siblings based on Wilcoxon rank-sum test.

Fig. 7: *ereb184* modulates pleiotropy in LA and TBN.
a) Feed-forward loops (FFLs) from the 'leaf' GRN are represented with *ereb184* in each of the node positions and number of times each occurs. The graph below shows GO terms overrepresented within the Z position when EREB184 is in the X position. **b)** An example of a sub-network from the 'leaf' GRN, which shows EREB184 participating in multiple FFLs with Knotted1-FFL highlighted *ereb184* connections to proximal-distal patterning genes that were detected in the leaf network as directly targeting *lg2*. The solid yellow arrows represent ChIP-seq validated connections. **c)** Genomic view of the intergenic space upstream (100 kb) and just downstream of *ereb184*. The tracks from top to bottom: nucleotide diversity (π), conserved non-coding sequences, multi-trait GWAS, unmethylated regions, leaf chromatin interaction data (Hi-C), structural variation, RNA-seq, and ATAC-seq. Data from public sources are indicated in Data Accessibility. **d)** The effect of structural variation (SV) presence/absence in the promoter region of *ereb184* across 231 accessions on LA and TBN traits, and the effect of SV on *ereb184* expression within 26 NAM founder lines.

Supplemental Note
This supplemental note along with references describes the biology behind the mutants that we are using in this study.
The *liguleless1 (lg1)* gene encodes a SQUAMOSA BINDING PROTEIN (SBP) TF and loss-of-function mutants completely abolish ligule and auricle formation, yet maintain a clear blade-sheath boundary (Moreno et al. 1997). In *liguleless2* (*lg2*) mutants, the blade-sheath boundary is more diffuse and reduced auricle tissue is retained at the leaf margins. This suggests that LG2, a bZIP TF, may be involved in defining the blade-sheath boundary (Walsh, Waters, and Freeling 1998) and that *lg1* is required for proper ligule differentiation (Harper and Freeling 1996).

During early tassel development, the indeterminate inflorescence meristem initiates a defined number of indeterminate axillary branch meristems at its flanks, which produce the long tassel branches, and then abruptly shifts to initiating short branches (Kellogg 2007). The *ramosa1* (*ra1*) gene, encoding a C2H2 TF specific to panicoid grasses, controls this process by imposing determinate fate on axillary meristems in a spatiotemporal manner (Vollbrecht et al. 2005). The RA1 protein accumulates adaxial to the base of axillary meristems that will produce short branches (Vollbrecht et al. 2005). Prior to RA1 expression, the LG1 protein accumulates in an overlapping domain at the base of the long branch meristems, but not the short ones, and RA1 can bind and negatively modulate *lg1* expression based on ChIP-seq and transcriptome studies (Eveland et al. 2014).

Since RA1 is an inflorescence-specific TF, its regulation of *lg1* is not present in developing ligules. Similarly, WAVY AURICLE BLADE1 (WAB1), a TCP family TF, is a tissue-specific factor that promotes expression of *lg1* in the tassel. In *Wab1* gain-of-function mutants, LG1 over-accumulates at the base of tassel branches resulting in wider branch ligulelessangles and is ectopically expressed in the leaf, causing aberrant ligule tissue in the sheath (Lewis et al. 2014). Loss-of-function *wab1* mutants (allelic to *branch angle defective1* (*bad1*)), have more upright tassel branches (Bai et al. 2012; Lewis et al. 2014). Another branching mutant, *ramosa2* (*ra2*), which encodes a LATERAL ORGAN BOUNDARY (LOB) domain TF (Bortiri et al. 2006), acts upstream of *wab1*/*bad1* and in a different pathway than *lg1* (Bai et al. 2012). Tassel branches of *ra2* mutants are very upright.

RNAi knockdown lines of the BR receptor kinase, BRASSINOSTEROID INSENSITIVE1 (BRI1), an initiator of BR signaling, and BR INSENSITIVE2 (BIN2), a GSK3-like kinase and negative regulator of BR transcriptional response, show opposite architectural phenotypes. The *bri1*-RNAi mutant significantly knocked down *zmbri1* expression as well as expression of four other paralogs, causing decreased BR signaling; ligule and auricles are abnormal and leaves were more upright, and more upright tassel branches (Vajk 2019). *bin2*-RNAi plants have wide open leaves due to expanded auricles and long, open tassel branches (Kir 2015).

mutants used in network analyses	**allele**
brassinosteroid insensitive2 (bin2)	*bin2*-RNAi
brassinosteroid insensitive1 (*bri1*)	*bri1*-RNAi
feminized, upright, narrow (*fun*)	*fun1-1*
liguleless1 (*lg1*)	*lg1-R*
liguleless2 (*lg2*)	*lg2-R*
ramosa1 (*ra1*)	*ra1-R*
ramosa2 (*ra2*)	*ra2-R*
wavy auricle blade1 (wab1)	*wab-rev, Wab-1* (dominant)

Extended Data Figures

Extended Data Fig. 1: Overview of biological samples collected for this study

Representative images of hand-dissected tassel primordia from B73 control plants at **A.** stage 1, which captures branch meristem initiation and **B.** stage 2, which captures branch outgrowth. Scale bars = 1,000 µm. **C.** Longitudinal section through the shoot apical meristem (SAM) of a B73 control plant depicting the microscopic view of the shoot apex to the right. In situ hybridization with a liguleless 1 (lg1) anti-sense probe marks developing ligules. Two sections from the shoot apex were sampled: shoot apex 1 includes the SAM and cells pre-patterned to be ligule and shoot apex 2 excludes the SAM and enriches for developed ligule. Leaf primordia are designated according to plastochron number (P). White arrow denotes the pre-ligular band while black arrows indicate the developing ligule on P7 and successive leaf primordia.

Extended Data Fig. 2: Principal component analysis of the expression dataset

The image shows the three principal components in 3-dimensional space of the entire transcriptional dataset (*n*=140) generated from the two tassel primordia developmental stages and shoot apex sections. Genotypes are marked by different colors and tissue type by different symbols. The principal component analysis was calculated based on the top 500 dynamically expressed protein-coding genes.

Extended Data Fig. 3: Dynamically expressed genes during tassel branching and ligule differentiation

A. Volcano plot showing variation in gene expression associated with tassel branch development based on comparing between tassel stages 1 and 2 in B73 normal plants. Genes expressed higher in stage 2 are in blue and those in yellow are decreasing in expression. **B.** Volcano plot representing variation in gene expression associated with ligule differentiation based on the comparison between the shoot apex 1 and 2 samples in B73 normal plants. Genes expressed higher in shoot apex 2 are in blue and those in yellow are decreasing in expression. Only genes with FDR < 0.05 are plotted along the x- (log2 fold change) and y- (-log 10 FDR) axis. Some classical maize genes are annotated.

Extended Data Fig. 4: Many genes are differentially expressed in two developmental contexts during tassel branch outgrowth and ligule differentiation

The heatmap displays relative gene expression profiles of annotated TFs and classical maize genes across both stages of tassel primordia and shoot apices sampled (n = 86). Genes were differentially expressed in the comparisons between tassel stages 1 and 2 and between shoot apex 1 and 2 with FDR < 0.05 (gray area of the Venn diagram). For each developmental context, DE genes that were up-regulated across developmental time are annotated with a blue box and down-regulated genes annotated with a yellow box.

Extended Data Fig. 5: Maize developmental marker genes correspond to meristem identity and determinacy shifts across the tassel developmental gradient

Expression trajectories of known maize developmental marker genes for meristem identity and determinacy are visualized to assess robustness of the five stage B73 normal tassel developmental gradient. **A.** Heatmap shows gene expression of selected maize inflorescence

markers across the five tassel primordia stages in B73. **B.** Peak expression of classical maize genes associated with each stage of meristem development in B73 is shown on the left, and expression profiles for these marker genes in *liguleless2* and *ramosa1* mutant backgrounds are shown on the right. The *bd1* profile is not shown in the mutants since it comes on after stage 2.

Extended Data Fig. 6: Differences in gene expression of BR mutants compared to B73 controls in stage 2 tassels

The ternary plot shows the relative expression of genes mis-expressed in common between the two BR mutants compared to B73 at stage 2. Each dot represents a gene and its coordinates indicate relative expression in the three genotypes.

Extended Data Fig 7: Eigengene trajectories of co-expression modules from 'tassel' and 'leaf' networks

The expression profile that best fits an average of all genes within a co-expression module is depicted as a Module Eigengene (ME). *For each co-expression module in the* **A.** 'tassel' and **B.** 'leaf' GCNs, MEs are depicted by dots in each sample. Each module showed a distinct expression profile, with certain modules characterized by peak expression at specific developmental stages and/or in certain mutant backgrounds.

Extended Data Fig. 8: Density plots representing empirical distributions in comparison to whole genome h^2 and TBN and LA h^2

A. TBN h^2. Above 0 density represents the null distribution (purple arrow shows the 95th percentile) in comparison to h^2 explained by the selected co-expressed network modules (orange arrow) and whole genome h^2 (green arrow). Below 0 density represents null distribution (purple arrow shows the 95th percentile) in comparison to h^2 explained by the combined network motif (orange arrow) and whole genome h^2 (green arrow). **B.** LA h^2. Upper panel represents the null distribution (purple arrow shows the 95th percentile) in comparison to h^2 explained by the selected co-expressed network modules (orange arrow) and whole genome h^2 (green arrow). Lower panel represents null distribution (purple arrow shows the 95th percentile) in comparison to h^2 explained by the combined network motif (orange arrow) and whole genome h^2 (green arrow)

Extended Data Fig. 9: Depiction of statistical genetic interactions predicted for *ereb184* with the top recurrent TFs within three-node network motifs

Based on makers within the genomic windows defined as ± 2 kb from the transcriptional start site (TSS) and transcriptional termination site (TTS) of *ereb184 and the recurrent TFs from 3-node motifs*, statistical genetic interactions were predicted. These interactions are represented as links between genes located on a circular visualization of the maize genome. Grey and tan links represent significant interactions for the traits TBN, LA and PhPC2. Tan links highlight statistical interactions that are supported by the GRN data.

Extended Data Fig. 10: Characterization of TBN and LA phenotypes in homozygous *zhd* mutant alleles
Homozygous mutant alleles of *zhd1-Mu227* and *zhd21-Mu8735* were compared to normal W22 (bz1-mum9) plants and showed no significant differences in **A**. tassel branch number (TBN) or **B**. leaf angle (LA). From left to right in both panels: *zhd1/1* (*n*=35); *zhd21/21* (*n*=24); +/+ (*n*=31). Wilcoxon rank-sum test is shown above each comparison.

Supplementary Tables
Supplementary Table 1: Gene expression in TPM across 140 RNA-seq samples.
Supplementary Table 2: DE genes with FDR < 5% derived from the comparison of B73 stage 2 tassel primordia vs. stage 1.
Supplementary Table 3: GO terms associated with DE genes derived from the comparison of B73 stage 2 tassel primordia vs. stage 1.
Supplementary Table 4: DE genes with FDR < 5% derived from the comparison of B73 shoot apex 2 vs. shoot apex 1.
Supplementary Table 5: GO terms associated with the DE genes derived from the comparison of B73 shoot apex 2 vs. shoot apex 1.
Supplementary Table 6: Genes that are DE between tassel stage 1 and stage 2 and shared between the BR mutants compared to B73 control.
Supplementary Table 7: Relative expression of genes commonly DE in the two BR mutants along the tassel stage 1 to stage 2 developmental gradient compared to the B73 control.
Supplementary Table 8: GO and TF enrichment analysis of genes commonly DE in the two BR mutants between tassel stage 1 and stage 2 development compared to the B73 control.
Supplementary Table 9: Summary of gene co-expression modules from the 'tassel' and 'leaf' context-specific networks.
Supplementary Table 10: Maize genes grouped based on the 'tassel' and 'leaf' gene co-expression modules.
Supplementary Table 11: Gene co-expression module preservation matrix between 'tassel' and 'leaf' networks.
Supplementary Table 12: GO terms overrepresented within 'tassel' and 'leaf' GCN modules.
Supplementary Table 13: GO terms overrepresented within 'tassel' and 'leaf' GCN preserved sub-modules.
Supplementary Table 14: TF enrichment analysis of the predicted regulators of *liguleless2* in the leaf GRN shown in Figure 2c.
Supplementary Table 15: i) Summary statistics of the three-node network motifs annotated in the GRNs. ii) Top one-hundred recurrent TFs within the three-node network motifs.
Supplementary Table 16: GEBVs and BLUPs of the elected Ames diversity lines.
Supplementary Table 17: Pearson correlations of phenotypic traits: Growing degree days to silking (GDD_DTS), Growing degree days to anthesis (GDD_DTA), Predicted GEBV of Tassel Branch Number (TBN predicted), Predicted GEBV of Leaf Angle (LA predicted); Predicted GEBV of the three principal components of LA, TBN, and ERN (PhPC1 predicted, PhPC2 predicted, PhPC3 predicted),TBN, LA, PhPC1, PhPC2.
Supplementary Table 18: i) Module-trait correlation of the sixteen modules identified in the comprehensive GCN. ii) maize genes grouped based on the comprehensive GCN modules.

Supplementary Table 19: Gene co-expression module heritabilities (h^2) for leaf angle (LA) and tassel branch number (TBN).
Supplementary Table 20: GWAS SNP-trait associations for LA, TBN, PhPC1 and PhPC2 from the single-trait approach using two sets of markers.
Supplementary Table 21: GO terms associated with genes proximal to significant SNP-trait associations from the single-trait GWAS for PhPC2.
Supplementary Table 22: Multi-trait GWAS SNP-trait associations for LA, TBN using two sets of markers.
Supplementary Table 23: Predicted direct gene targets of EREB184 and ZHD21 in the 'leaf' GRN.
Supplementary Table 24: Statistical genetic interaction predictions between *ereb184 and* top recurrent TFs within three-node network motifs.
Supplementary Table 25: Single-trait GWAS results for LA based markers subset around sorghum orthologs of the highly connected three-node motifs in the maize networks.
Supplementary Table 26: GO terms associated with genes in position Z of *ereb184*-controlled FFLs in the 'leaf' network.

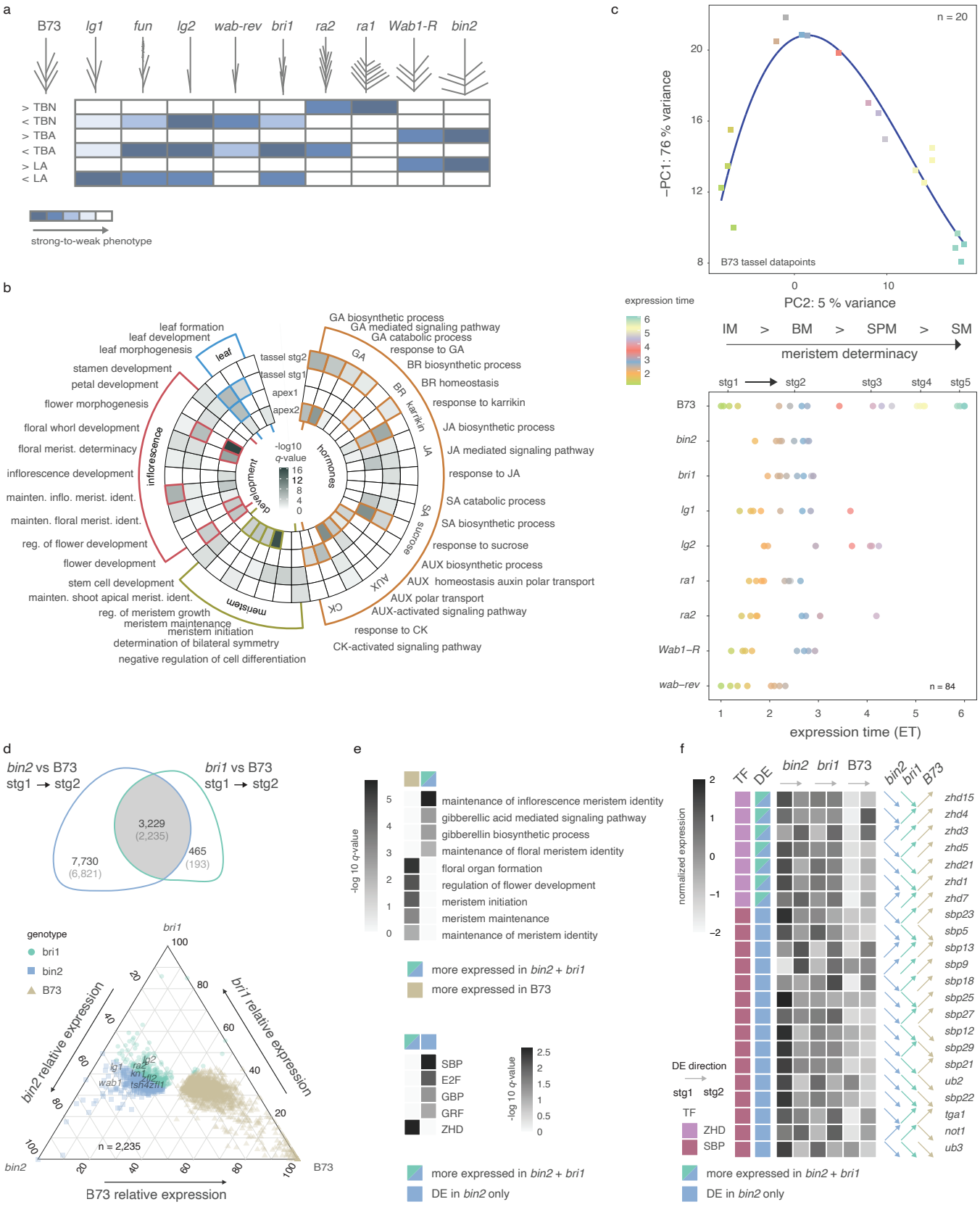

Fig.1: Transcriptional analyses across maize mutants with defects in leaf angle and tassel branching. **a**) Panel of maize mutants used in this study depicting unique tassel branching phenotypes compared to B73 controls. Color scale in the heatmap below indicates severity of tassel branch number (TBN), tassel branch angle (TBA) and leaf angle (LA) phenotype deviations from B73 controls; dark blue-to-white is strong-to-weak phenotype. **b**) Enrichment of GO terms associated with differentially expressed (DE) gene sets identified during the shift from stage 1 to stage 2 tassels and from shoot apex 1 to shoot apex 2. **c**) A 2-dimensional section of the first and second PC from the normal B73 tassel developmental gradient (n=20). The blue line represents the b-spline fit with ...

Fig.1... three degrees of freedom modeled within the dataset and used to classify samples relative to their developmental progression coded as expression time (ET). Squared dots represent the 20 tassel samples in ET. The underlying dot plot represents stages 1 and 2 tassel primordia from the different mutant backgrounds. Mutant data points are color-coded relative to B73 ET. The black arrow represents stages of meristem development along normal tassel developmental time: inflorescence meristem (IM), branch meristem (BM), spikelet pair meristem (SPM), spikelet meristem (SM). **d**) Venn diagram shows genes that are DE between tassel primordia at stage 1 and 2 in *bri1-RNAi* and *bin2-RNAi* mutants compared to B73 controls. Those with higher variation in expression at stg1 are shown in parentheses. The ternary plot below shows the relative expression of genes mis-expressed in common between the two mutants compared to B73 at stage 1. Each dot represents a gene and its coordinates indicate relative expression in the three genotypes. Some examples of classical maize genes are noted. **e**) The top heatmap shows GO terms enriched among DE gene sets commonly expressed either higher or lower in the BR mutants compared to B73 controls in stage 1 tassels (from the ternary plot in **d**); the bottom heatmap shows overrepresented TF classes among genes expressed higher in *bri1* and *bin2* mutants at stage 1 and those expressed higher in bin2 only compared to B73 controls. **f**) Relative gene expression trends are shown for ZHD and SBP TF family members that were expressed higher in *bin2* and/or *bri1* mutants compared to B73 controls at stage 1.

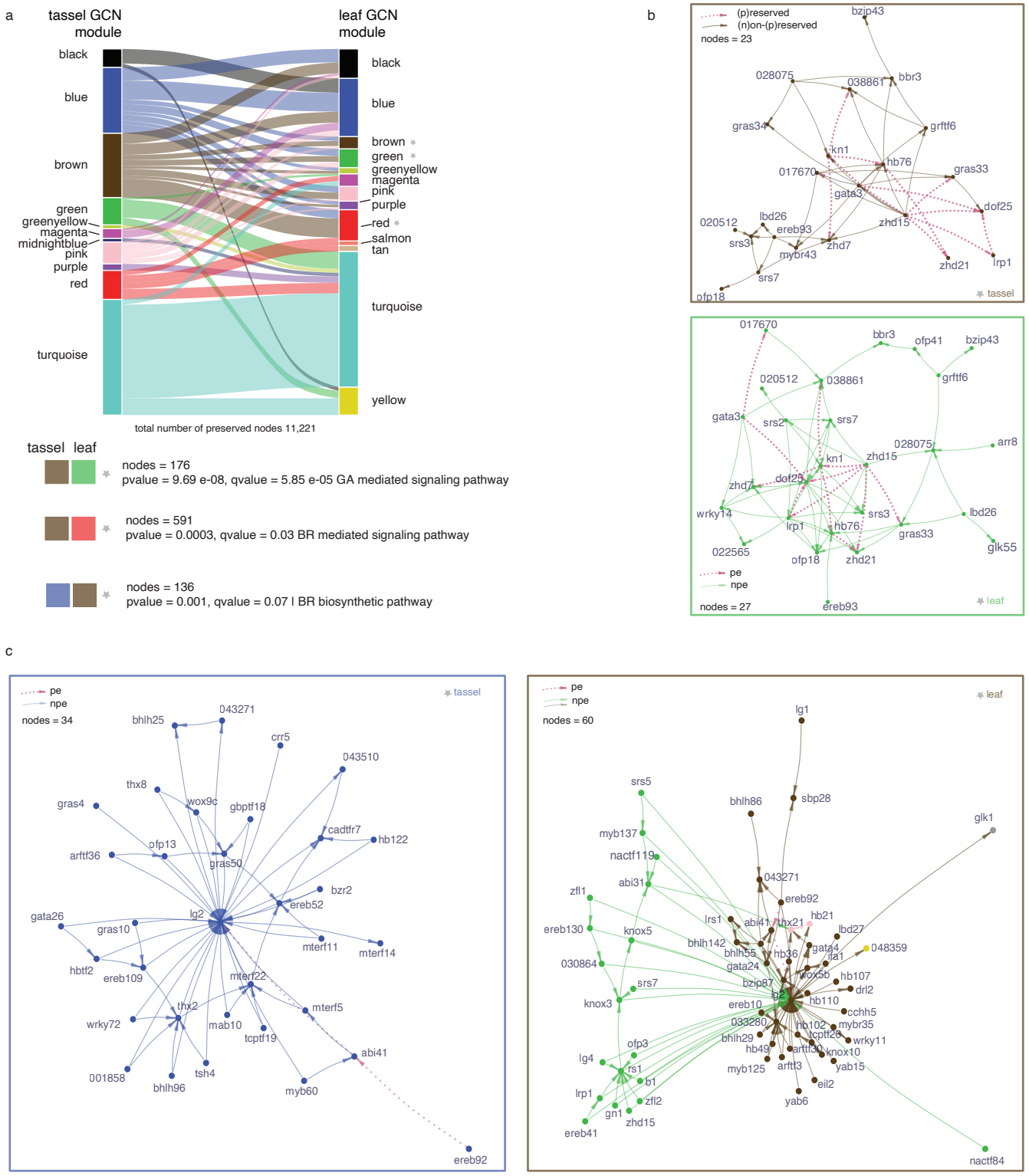

Fig.2: Conserved and divergent network connections between tassel and leaf gene regulatory networks. **a**) Gene co-expression network (GCN) preservation between 'tassel' and 'leaf' networks. Preserved modules are indicated by color and connected by lines (width is proportional to number of preserved genes). Colored boxes beneath the plot represent selected (starred) preserved gene regulatory sub-modules. Number of nodes in each preserved sub-module is indicated. **b**) Topological graph representation of preserved TFs in the 'tassel'-'leaf' "brown-green" sub-module based on data from GCN (edge weight) and gene regulatory network (GRN; edge directionality). Pink edges represent preserved regulatory connections and brown or green edges represent the network-specific wires. **c**) Topological graph representation of closest TF neighbors to *liguleless2* (*lg2*) in the 'tassel' and 'leaf' networks based on data from GCN (edge weight) and GRN (edge directionality). Pink edges represent preserved connections and blue or brown/green edges represent network-specific wires. The edge length is proportional to the weight of gene co-expression. Maize gene labels are from MaizeGDB or AGPv4 as Zm00001d[(6)].

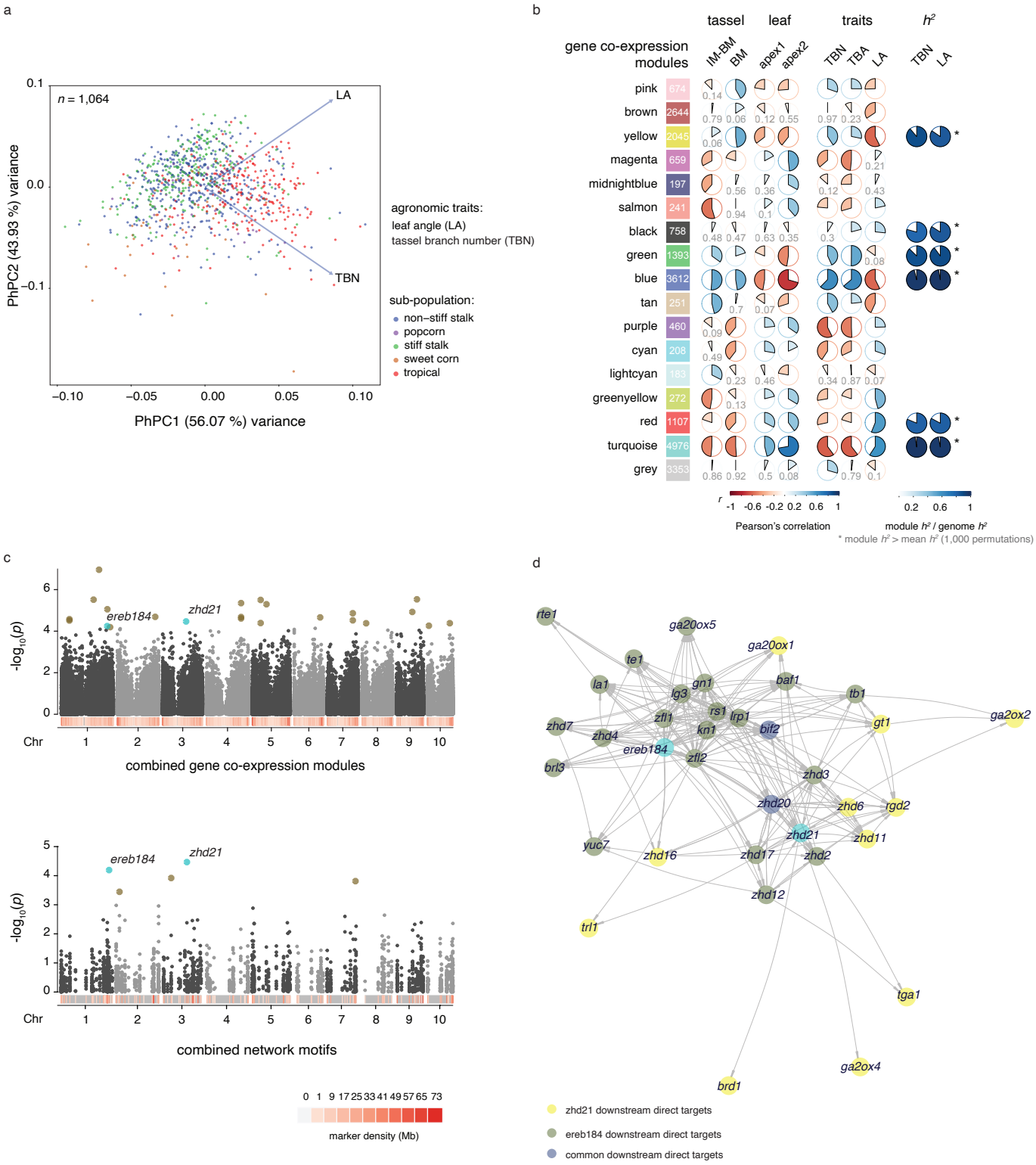

Fig.4: Multi-trait GWAS detected candidate pleiotropic genes for LA and TBN.
a) Phenotypic Principal Components (PhPCs) of Leaf Angle (LA) and Tassel Branch Number (TBN). Individuals are plotted according to their PhPC1 scores of LA and TBN on the x-axis and their PhPC2 scores on the y-axis. The percentage of total variance explained by a component is listed in parentheses on the axis. Blue arrows represent trait loadings for a given PhPC where its direction on the x-axis represents its contribution to PhPC1 and direction on the y-axis, its contribution to PhPC2. Subpopulations are color-coded and grouped according to PhPCs. **b**) Analysis of module-trait relationships for the combined gene co-expression network. Modules are represented as colored boxes with the number of co-expressed genes indicated. The correlogram to the right represents the module trait relationship where shades of blue and red represent positive and negative Pearson's correlation, respectively, with darker color indicating a stronger positive or negative correlation. Modules representing more than 80% of the whole genome heritability (h^2) for TBN and LA are indicated. **c**) Multi-trait GWAS results ...

Fig.4:... using subsets of markers within 2 kb proximity of genes in the six co-expression modules with significant h^2 in panel **b** (top) and in the top 200 interconnected TFs within three-node motifs from Fig. 3b. Brown and blue dots represent significant SNP-trait associations; blue dots indicate loci identified in both analyses. **d**) Topological graph representation of a sub-network including *ereb184*, *zhd21* and their predicted downstream target genes based on data from the 'leaf' GRN (edge directionality).

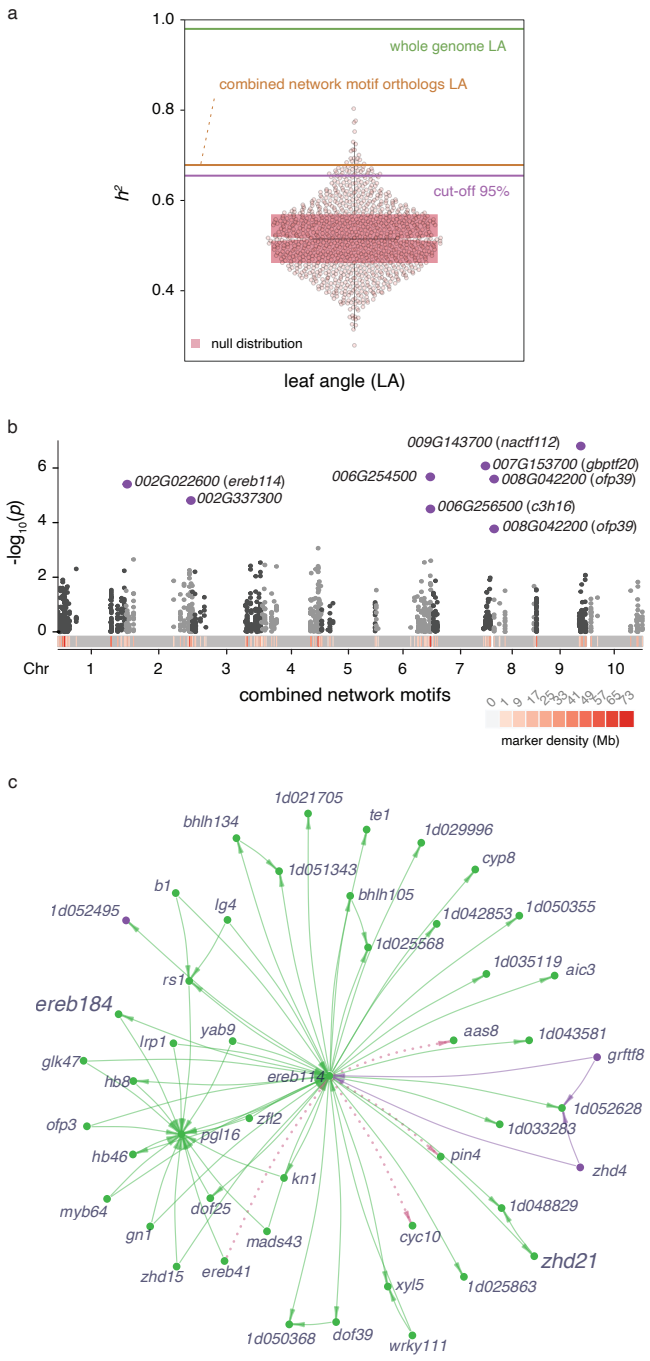

Fig.5: GWAS for LA in sorghum using biological information derived from maize.
a) LA narrow-sense heritability of 158 sorghum-maize syntenic orthologs in comparison to a null distribution (violin plot). Purple line represents 95% cut-off, orange line represents LA h^2 of the sorghum orthologs, green line is the whole genome LA h^2. **b**) Manhattan plot showing GWAS results for LA based on markers in proximity of the 158 sorghum-maize syntenic orthologs. Purple dots represent significant SNP-trait associations for LA. **c**) Topological graph representation of *ereb114* and its closest network neighbors in the maize 'leaf' GCN (edge weight) and GRN (edge directionality). Green and purple nodes and edges are colored based on module assignment in the 'leaf' GCN. Pink edges represent preserved connections with the 'tassel' GCN. Edge length is proportional with the gene co-expression weight.

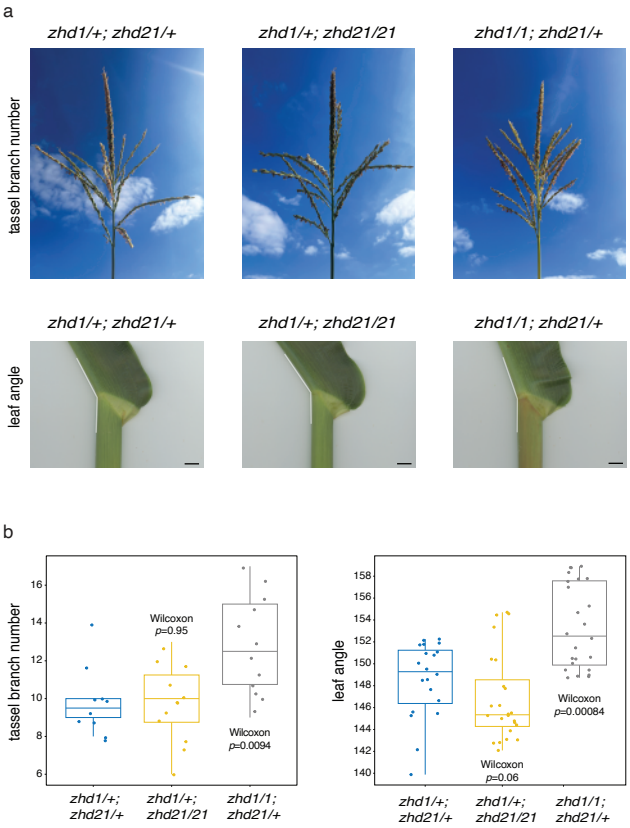

Fig. 6: Characterization of pleiotropic phenotypes from combining *zhd* mutant alleles.
a) Representative tassel branch and leaf angle phenotypes resulting from genetic interactions between mutant alleles of *zhd1* and *zhd21*, from left to right: *zhd1/+;zhd21/+*, *zhd1/+;zhd21/zhd21*, *zhd1/1;zhd21/+*. Black bar = 1cm. **b**) Among combinations of mutant alleles, *zhd1/1;zhd21/+* showed significant differences in TBN and LA from the zhd1/+;zhd21/+ normal siblings based on Wilcoxon rank-sum test.

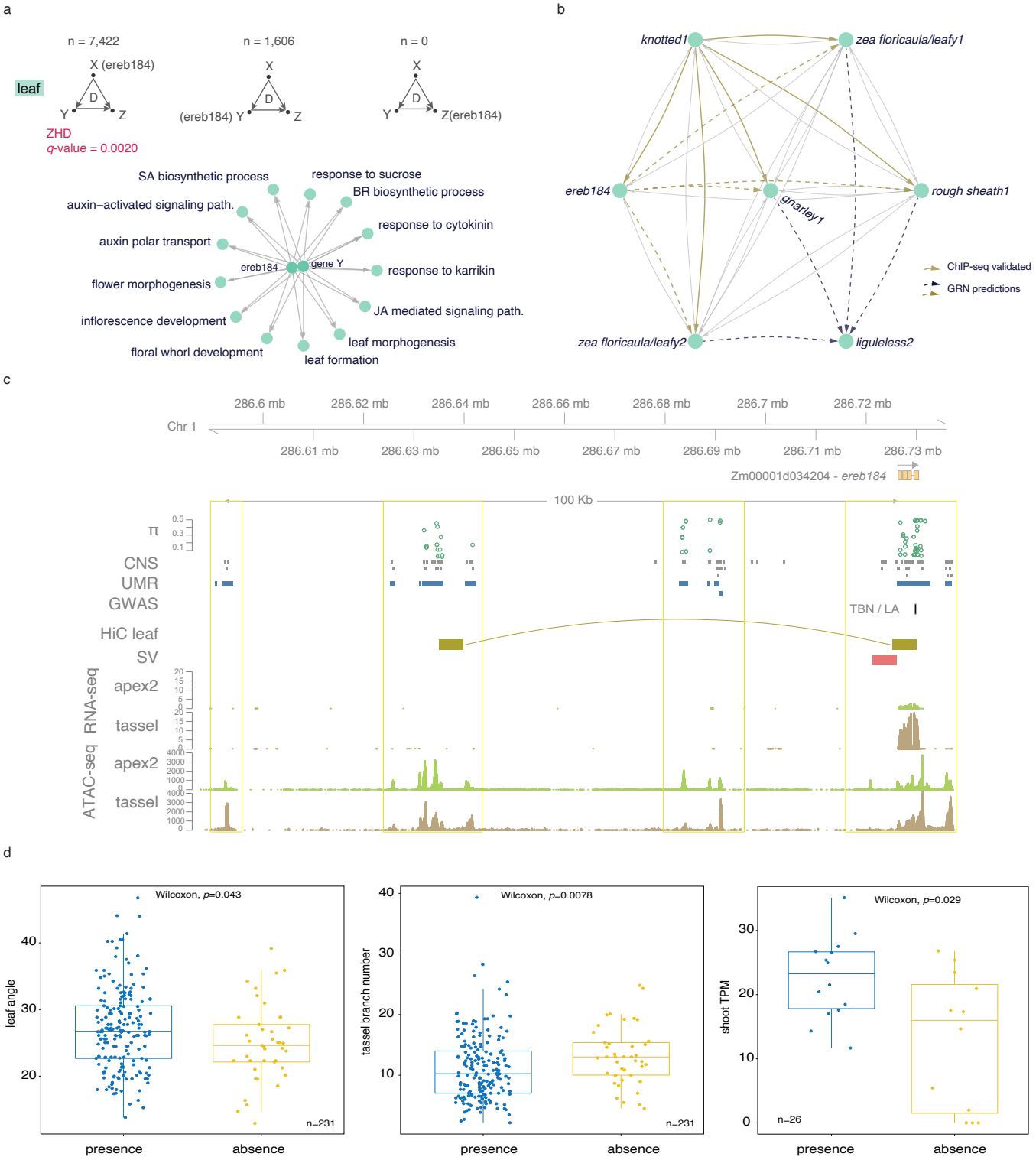

Fig.7: *ereb184* modulates pleiotropy in LA and TBN.

a) Feed-forward loops (FFLs) from the 'leaf' GRN are represented with *ereb184* in each of the node positions and number of times each occurs. The graph below shows GO terms overrepresented within the Z position when EREB184 is in the X position. **b**) An example of a sub-network from the 'leaf' GRN, which shows EREB184 participating in multiple FFLs with Knotted1-FFL highlighted *ereb184* connections to proximal-distal patterning genes that were detected in the leaf network as directly targeting *lg2*. The solid yellow arrows represent ChIP-seq validated connections. **c**) Genomic view of the intergenic space upstream (100 kb) and just downstream of *ereb184*. The tracks from top to bottom: nucleotide diversity (π), conserved non-coding sequences, multi-trait GWAS, unmethylated regions, leaf chromatin interaction data (Hi-C), structural variation, RNA-seq, and ATAC-seq. Data from public sources are indicated in Data Accessibility. **d**) The effect of structural variation (SV) presence/absence in the promoter region of ereb184 across 231 accessions on LA and TBN traits, and the effect of SV on *ereb184* expression within 26 NAM founder lines.